Geophys. J. Int. (2004) **157,** 1316–1330 doi: 10.1111/j.1365-246X.2004.02271.x

Determination of regional stress tensors from fault-slip data

Peiliang Xu

Disaster Prevention Research Institute, Kyoto University, Uji, Kyoto 611-0011, *Japan. E-mail: pxu@rcep.dpri.kyoto-u.ac.jp*

Accepted 2004 January 16. Received 2004 January 13; in original form 2001 December 28

SUMMARY

Stress tensors are regularly determined from fault-slip and/or earthquake focal mechanism data in structural geology and seismotectonics. The inverse problem is non-linear, unless empirical rules of rupture and friction are employed. All the methods used to date to determine the stress tensor to this non-linear inverse problem are of a local nature, and thus cannot guarantee that the global optimal stress tensor has been obtained. We apply a hybrid global optimization method to find the global optimal stress tensor. Although the inverse problem is non-linear, the effect of non-linearity on the biases of stress tensors has not been investigated. We will examine the biases of inverted stress tensors and their effect on the principal orientations of stress and the shape parameter of the stress ellipsoid. The biases of stress parameters have been shown to be comparable with the estimated stress parameters numerically. We compare the accuracy of the four stress parameters, with and without taking the errors in fault planes into account. If the errors in fault planes are not taken into account, the stress parameters are too optimistically estimated by a factor of 4 to 9 in the example. We will also mathematically reformulate the assumption that the directions of maximum shear stress represent those of slips on fault planes as two functionally independent but equivalent constraints of equality. The new formulation is computationally more effective and provides a correct method for calculating the accuracy of stress parameters.

Key words: global optimization, non-linear inversion, stress.

1 INTRODUCTION

Knowledge of the state of stress in the Earth's crust and upper mantle is important in the Earth sciences, to understand geological structure, plate motion and plate tectonics, for instance. Earthquakes are one of the most obvious manifestations of stress. Wallace (1951) investigated the relationships among faults, maximum shear stress and slip on fault planes, showed how to use graphical methods to determine the orientations of the maximum shear stress, and concluded that the orientations and nature of the stress system can be determined from a set of fault planes and associated slip vectors. Bott (1959) further developed a mathematical model in order to deal with faults of all kinds by assuming that the direction of slip/striae on the fault plane represents the direction of maximum shear stress on the fault. The theoretical analysis by Wallace (1951) and Bott (1959) is significant in providing a mathematical model to connect fault planes and striae to the causative stress tensor and is now well-known as the Wallace–Bott model. Under an extra assumption that one of the nodal planes can be unambiguously identified as the fault plane, McKenzie (1969) was able to establish a relation between earthquake focal mechanisms and the stress tensor, which is essentially the same as that of Bott (1959) but is important for the computation of stress tensors from earthquake focal mechanisms. Among many applications of stress tensor inversion, we mention the World Stress Map project (Zoback 1992).

Following the pioneering theoretical analysis by Wallace (1951) and Bott (1959), and after the first practical attempt to determine regional stress or palaeostress tensors from fault plane and striae data by Carey & Brunier (1974), studies of stress tensor inversion may be classified into three major categories. First, a number of methods have been proposed to reduce or eliminate the effect of outliers on the stress tensor (Gephart & Forsyth 1984; Will & Powell 1991) and to deal with heterogeneous data (see e.g. Angelier & Manoussis 1980; Huang 1988; Wyss & Lu 1995; Albarello 2000; Yamaji 2000). Second, keeping in mind that only a reduced deviatoric stress tensor can be found from fault planes and slip/striae directions, Angelier (1989) used empirical relations pertaining to rupture, friction and depth to constrain the principal stresses and orientations, and showed that the full stress tensor can be completely determined with these extra constraints. Graphical methods were also designed to determine the orientations of a stress tensor (e.g. Lisle 1992). The disadvantage of graphical methods is twofold: (i) the orientations of the stress tensor can only be conveniently represented as areas on the unit sphere and (ii) the shape parameter of the stress ellipsoid cannot be produced. Graphical methods can, however, be used to help separate heterogeneous data sets in some cases (e.g. Fry 1999). For an excellent review on some of these and other methods, the reader is referred to Angelier (1994).

Inversion of stress tensors from fault-slip or earthquake focal mechanism data is non-linear, unless additional prior assumptions

are imposed on the magnitudes of shears (Michael 1984) or empirical rules of rupture and friction are used to linearly constrain the three principal stresses (Angelier 1989). It should be noted that if earthquake focal mechanisms are used to invert for stress tensors, one has to either first distinguish the true fault plane from the auxiliary plane (see e.g. Ellsworth & Xu 1980) or resort to some special estimation techniques so that the true fault planes can be automatically selected in the process of inversion (e.g. Gephart & Forsyth 1984). For an excellent description of inverting stress from earthquake focal mechanisms, the reader is referred to a recent paper by Angelier (2002). Angelier (2002) also proposed an inversion technique which does not need to distinguish between two nodal planes. In order to obtain the global optimal stress tensor that best fits the data, two strategies are commonly employed: (i) use the Monte Carlo method to sample a number of points in the space of stress tensors, and then choose the best possible point from the samplings and start applying a local optimization algorithm to find a solution (see e.g. Etchecopar *et al.* 1981; Angelier *et al.* 1982); and (ii) use the grid method to find a solution (see e.g. Gephart & Forsyth 1984; Xu *et al.* 1992; Horiuchi *et al.* 1995; Yamaji 2000). These types of methods have been reported to fail to find the globally optimal stress tensor $\hat{\boldsymbol{T}}$, unless the initial point is in a small neighbourhood of $\hat{\boldsymbol{T}}$ or the gridding is made sufficiently fine (see e.g. Etchecopar *et al.* 1981; Angelier *et al.* 1982; Gephart & Forsyth 1984). How to find the globally optimal stress tensor provides the first motivation for this work.

Statistical assessment of the estimated stress tensor is almost as important as finding the optimal solution itself. Angelier *et al.* (1982) first estimated both the fault-slip parameters and the reduced stress tensor simultaneously, and took errors in both the fault planes and the slip vectors into account for the computation of accuracy. Gephart & Forsyth (1984) used the L_1-norm to simultaneously estimate the fault plane parameters and the stress tensor. Yin & Ranalli (1993) proposed a probabilistic model to deal with errors of the fault planes and slips from the point of view of directional statistics. Choi *et al.* (1996) did a large-scale simulation to investigate the effect of random errors in fault planes and slips on the stress tensor solutions and the cost functions. If the probabilistic distribution of the estimated stress tensor is known, one can then conduct a rigorous statistical analysis of the tensor (Xu 1999). Michael (1987) and Albarello (2000) used bootstrap resampling to estimate the confidence region of the reduced tensor and to test the assumption of stress uniformity. As noted above, the observational model of fault-slips with respect to the stress tensor is non-linear. On the other hand, the fault plane uncertainties are propagated in determining the stress tensor. Furthermore, the mapping from the stress tensor to the principal stresses and their directions is non-linear as well. From a statistical point of view, the non-linearity in the observational model and tensor mapping biases the estimated stress tensor. To date, the issue of bias has never been investigated, although the issue of confidence regions for the estimated reduced stress tensor has been well addressed by Angelier *et al.* (1982), Gephart & Forsyth (1984), Michael (1987) and Yin & Ranalli (1993), among others. We will use the bias analysis approach of Box (1971) to investigate the biases of the estimated stress tensor from fault-slip and/or earthquake focal mechanism data. A statistical analysis of stress tensors provides the second motivation for this work.

The purpose of this paper is twofold: (i) we will apply the non-linear optimization method of Xu (2002, 2003a,b) to determine the stress tensor from fault-slip and/or earthquake focal mechanism data. Unlike the local iterative and grid methods, our method will always correctly produce the global optimal stress tensor; (ii) we will investigate the bias and accuracy of the estimated stress tensor, due to the non-linearity of slip directions with respect to fault-slip measurements and the maximum shear stress direction with respect to the reduced deviatoric stress tensor, mapping into the eigenspace, and the multiplicative nature of noise of the fault planes. The paper is organized as follows. In Section 2, we will briefly outline the principle for inverting stress tensors from fault-slip data. It will then become clear that for each fault-slip pair, there are two independent constraints among the fault plane parameters, the slip direction and the reduced stress tensor. Angelier *et al.* (1982) used one independent but mathematically equivalent constraint for each pair of fault-slip data in the simultaneous estimation of stress tensors and fault-slip parameters (see also Will & Powell 1991). As will be seen later, a direct consequence of using the equivalent constraint for each fault is that the accuracy of the estimated stress parameters is incorrectly computed. Gephart & Forsyth (1984) also used one constraint only (see also McKenzie 1969; Gephart 1990). However, unlike Angelier *et al.* (1982), this constraint will be shown later to not be mathematically equivalent to the assumptions of Wallace (1951) and Bott (1959). Thus, strictly speaking, the method of Gephart & Forsyth (1984) is not a simultaneous estimation technique in the sense of Angelier *et al.* (1982). Section 3 will discuss the solutions to the inverse problem. First we will provide an alternative formulation to simultaneously estimate the fault-slip parameters and the reduced stress tensor. Then we will focus on the inverse problem of stress tensors with four parameters, since this formulation has been widely used by most of researchers. In Section 4, we will work out the statistical measures of bias and accuracy for the inverted stress tensor, with and without taking the errors of fault planes into account. Since the errors in fault planes and slips are not necessarily small, we will derive the accuracy measure of higher orders as well. Section 5 will summarize an example of the practical implementation of the new solution strategy and the computation results.

2 THE PRINCIPLE FOR INVERTING STRESS TENSORS

Inversion of stress tensors involves the following three basic elements: fault planes, slip vectors on the fault planes, and stress tensors. A fault plane is completely specified by two angles: the fault strike ϕ defined as the azimuth of the strike direction in seismology and the dip δ defined as the angle between a horizontal plane and the fault plane. With respect to a reference system in which the x-axis points north, the y-axis points east and the z-axis points upwards (Fig. 1), the outward normal $\mathbf{n}$ to the fault plane can be described by its three components:

$$n_x = -\sin\delta\sin\phi, \tag{1a}$$

$$n_y = \sin\delta\cos\phi, \tag{1b}$$

$$n_z = \cos\delta. \tag{1c}$$

The direction of a slip on a fault plane is conveniently described by the *rake*, which is the angle λ between the slip and strike directions. The unit slip vector $\mathbf{s}$ is then given as:

$$s_x = \sin\lambda\cos\delta\sin\phi + \cos\lambda\cos\phi, \tag{2a}$$

$$s_y = -\sin\lambda\cos\delta\cos\phi + \cos\lambda\sin\phi, \tag{2b}$$

$$s_z = \sin\lambda\sin\delta. \tag{2c}$$

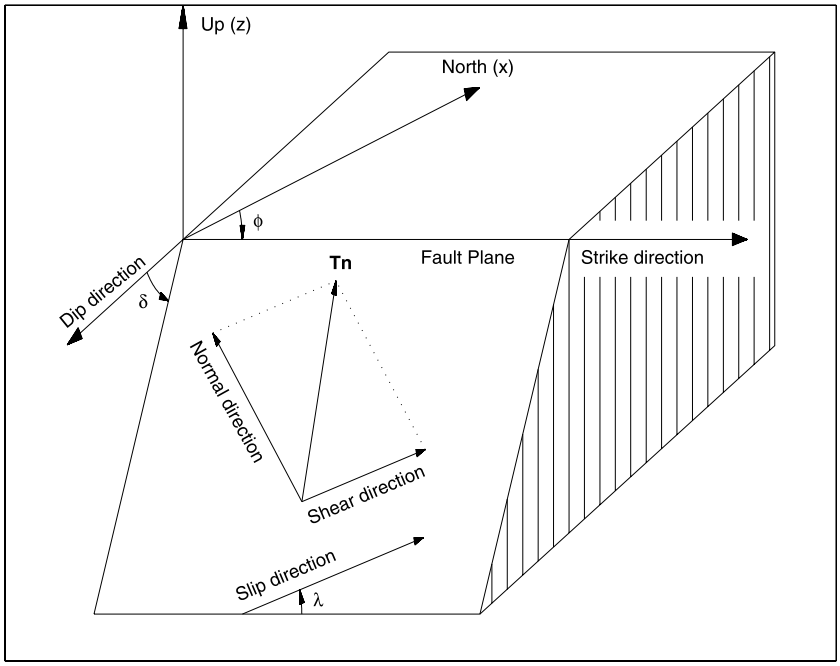

Figure 1. Geometrical illustration of fault planes, slip directions, the normal direction to the fault plane, and the directions of the normal and shear stresses on the fault plane. The slip vector is the movement of the hanging wall block relative to the footwall block (shown in this figure). Note that the traction **Tn** is not on the fault plane.

The normal and slip unit vectors (1) and (2) can also be derived by transforming the corresponding formulae in Angelier *et al.* (1982) and Koyama (1997) into our coordinate system.

As the first assumption for determining stress tensors from fault-slip data, we assume that the stress tensor $\boldsymbol{T}$ is symmetric. The traction vector $\boldsymbol{\sigma}$ acted on the fault plane by $\boldsymbol{T}$ can be computed as follows:

$$\boldsymbol{\sigma} = \boldsymbol{T}\mathbf{n}. \tag{3}$$

By projecting $\boldsymbol{\sigma}$ onto the fault plane, we obtain the component of $\boldsymbol{\sigma}$ on the fault plane:

$$\boldsymbol{\tau}_s = \boldsymbol{\sigma} - \mathbf{n}^T\boldsymbol{\sigma}\mathbf{n} = \boldsymbol{T}\mathbf{n} - (\mathbf{n}^T\boldsymbol{T}\mathbf{n})\mathbf{n}, \tag{4}$$

(see e.g. Etchecopar *et al.* 1981; Angelier *et al.* 1982), where $\mathbf{n}^T$ stands for the transpose of $\mathbf{n}$. $\boldsymbol{\tau}_s$ is better known as (resolved) *shear stress*. In the Earth sciences, two different conventions of sign have been used to represent the stress tensor $\boldsymbol{T}$. The first convention of sign conforms with that generally used in elasticity, in which tensions are positive and compressions negative (e.g. Lay & Wallace 1995; Ramsay & Lisle 2000). The second convention of sign is more often used in rock mechanics, with tensions defined as negative and compressions as positive (e.g. Amadei & Stephansson 1997; Mandl 2000). In the second case, (3) and (4) become

$$\boldsymbol{\sigma} = -\boldsymbol{T}\mathbf{n}$$

and

$$\boldsymbol{\tau}_s = -\boldsymbol{T}\mathbf{n} + (\mathbf{n}^T\boldsymbol{T}\mathbf{n})\mathbf{n}$$

respectively.

Although the shear stress $\boldsymbol{\tau}_s$ has been represented mathematically, we are still not able to determine the stress tensor $\boldsymbol{T}$ since $\boldsymbol{\tau}_s$ is not directly observable. It is physically reasonable to believe that the shear stress $\boldsymbol{\tau}_s$ must be related to the slip $\mathbf{s}$, although such relationships may be complex. The simplest relation assumes that the direction of shear stress $\boldsymbol{\tau}_s$ is the same as that of slip $\mathbf{s}$ (Wallace 1951; Bott 1959), which comprises the second assumption used in determining stress tensors from fault-slip data. Normalizing $\boldsymbol{\tau}_s$ as

$$\mathbf{f}_{sn} = \boldsymbol{\tau}_s/\|\boldsymbol{\tau}_s\| = \{\boldsymbol{T}\mathbf{n} - (\mathbf{n}^T\boldsymbol{T}\mathbf{n})\mathbf{n}\}/\|\boldsymbol{T}\mathbf{n} - (\mathbf{n}^T\boldsymbol{T}\mathbf{n})\mathbf{n}\|, \tag{5}$$

and equating it to the slip vector by using the second assumption, we obtain

$$\mathbf{s} = \mathbf{f}_{sn} = \{\boldsymbol{T}\mathbf{n} - (\mathbf{n}^T\boldsymbol{T}\mathbf{n})\mathbf{n}\}/\|\boldsymbol{T}\mathbf{n} - (\mathbf{n}^T\boldsymbol{T}\mathbf{n})\mathbf{n}\|, \tag{6}$$

where $\|\mathbf{x}\|$ is the length of $\mathbf{x}$. Alternatively, Michael (1984) first assumed that the slip vector $\mathbf{s}$ can be transformed into the maximum shear stress and then equated it to $\boldsymbol{\tau}_s$. Obviously, in addition to the condition (6), the method of Michael (1984) introduced one more assumption that a slip vector can be linearly converted into a force. It has been shown that (6) can be erroneous in highly fractured zones with complex faulted systems, due to kinematic interaction among faults (Dupin *et al.* 1993; Pollard *et al.* 1993; Nieto-Samaniego & Alaniz-Alvarez 1997).

We rewrite the stress tensor $\boldsymbol{T}$ as

$$\boldsymbol{T} = t_s\boldsymbol{D} + t_v\mathbf{I}, \tag{7}$$

where t_s and t_v are two scalar parameters, $\boldsymbol{D}$ is a symmetric deviatoric stress tensor specified by four unknown parameters, $\mathbf{I}$ is an identity matrix. Inserting (7) into (6) yields

$$\mathbf{s} = \{\boldsymbol{D}\mathbf{n} - (\mathbf{n}^T\boldsymbol{D}\mathbf{n})\mathbf{n}\}/\|\boldsymbol{D}\mathbf{n} - (\mathbf{n}^T\boldsymbol{D}\mathbf{n})\mathbf{n}\|, \tag{8}$$

which is the starting equation for stress tensor inversion. It is obvious from (8) that the slip direction $\mathbf{s}$ contains no information on the isotropic component and absolute magnitude of the stress tensor $\boldsymbol{T}$. We can only hope to determine the scale-free deviatoric stress tensor $\boldsymbol{D}$ from fault-slip data. $\boldsymbol{D}$ is often referred to as the *reduced stress tensor* in the literature. The most widely used four-parameter

representation of $\boldsymbol{D}$ is as follows:

$$\boldsymbol{D} = \begin{bmatrix} \cos\varphi & \alpha & \gamma \\ \alpha & \cos(\varphi + 2\pi/3) & \beta \\ \gamma & \beta & \cos(\varphi + 4\pi/3) \end{bmatrix} \tag{9}$$

(e.g. Angelier 1979, 1984; Angelier *et al.* 1982). Once the deviatoric tensor $\boldsymbol{D}$ is estimated, one can compute its three principal stresses $d_1 \geq d_2 \geq d_3$ and their directions which correspond to the principal stress directions of $\boldsymbol{T}$ also. One can also use the inversion results to compute a single magnitude parameter of the stress ellipsoid, defined as

$$R = \frac{d_1 - d_2}{d_1 - d_3}, \tag{10}$$

where $0 \leq R \leq 1$.

If each fault corresponds to one different stress tensor, then no inversion can be possible. As the third assumption for determining stress tensors from fault-slip data, we assume that the stress state that governs slips on a set of fault planes is uniform. As a consequence of this assumption, the total number of unknown stress parameters is reduced to four. In practical applications, one has to first classify data, which can generally be heterogeneous (Angelier & Manoussis 1980; Huang 1988; Yamaji 2000). For example, given a set of faults/striae, we must first check whether they should be clustered into a number of subsets, and as a result, decide a proper area and time span for each subset of data. This pre-processing or classification of data may help resolve the different geophysical interpretations of the same data set (compare Hardebeck & Hauksson 1999; Townend & Zoback 2001). Thus on the basis of these three assumptions, and if sufficient fault-slip data are collected, we can reconstruct the causative stress state using the least-squares method or other criteria.

2.1 Further discussions on the second assumption

Assume two unit vectors $\mathbf{u}_A$ and $\mathbf{u}_B$ on the unit sphere (Fig. 2). $\mathbf{u}_A$ and $\mathbf{u}_B$ will point to the same direction, if and only if all the three components of $\mathbf{u}_A$ and $\mathbf{u}_B$ are equal to each other. $\mathbf{u}$ has only two degrees of freedom however, since $\|\mathbf{u}\| = 1$. One method of representing $\mathbf{u}$ is to use two independent variables, longitude and latitude, for example. Thus we can rewrite the three-component equations $\mathbf{u}_A = \mathbf{u}_B$ as the following two equivalent but independent equations:

$$\lambda_A = \lambda_B, \tag{11a}$$

$$\phi_A = \phi_B. \tag{11b}$$

Comparing $\mathbf{u}_A$ and $\mathbf{u}_B$ to the slip vector $\mathbf{s}$ and the normalized unit vector $\mathbf{f}_{sn}$ respectively, we can readily obtain two functionally independent constraints of equality from (8) in the four stress parameters of $\boldsymbol{D}$ for each pair of fault-slip data, as in (11). To emphasize the dependence of (11) on fault-slip data and the four stress parameters, we can directly rewrite the two independent constraints of equality as follows:

$$\lambda_s(\delta, \phi, \lambda) = \lambda_f(\delta, \phi, \boldsymbol{D}), \tag{12a}$$

$$\phi_s(\delta, \phi, \lambda) = \phi_f(\delta, \phi, \boldsymbol{D}), \tag{12b}$$

for each pair of fault-slip data. Here the subscripts s and f denote the unit vectors $\mathbf{s}$ and $\mathbf{f}_{sn}$, respectively.

Instead of fully implementing the second assumption proposed by Wallace (1951) and Bott (1959), McKenzie (1969) and Gephart & Forsyth (1984), among others, have used only part of the information inherent in the second assumption, or more specifically the parallel condition of shear stress and slip directions. As a consequence, only one independent constraint can be derived. This single constraint is not equivalent to (11) mathematically, however. We note that some authors use the term *parallel* to mean exactly eqs (12) (e.g. Michael 1984).

More generally, let us assume that there exists ambiguity in the sense of slip. In other words, we do not know which angle, λ or $(\lambda \pm 180^\circ)$, is correct to represent the direction (sense) of slip. We will now show that even in this case of ambiguity, we should still derive two independent constraints of type (12). As the first step, we can reformulate λ and $(\lambda \pm 180^\circ)$ as two quasi-observables, one for the correct and the other for the erroneous sense of slip, and then

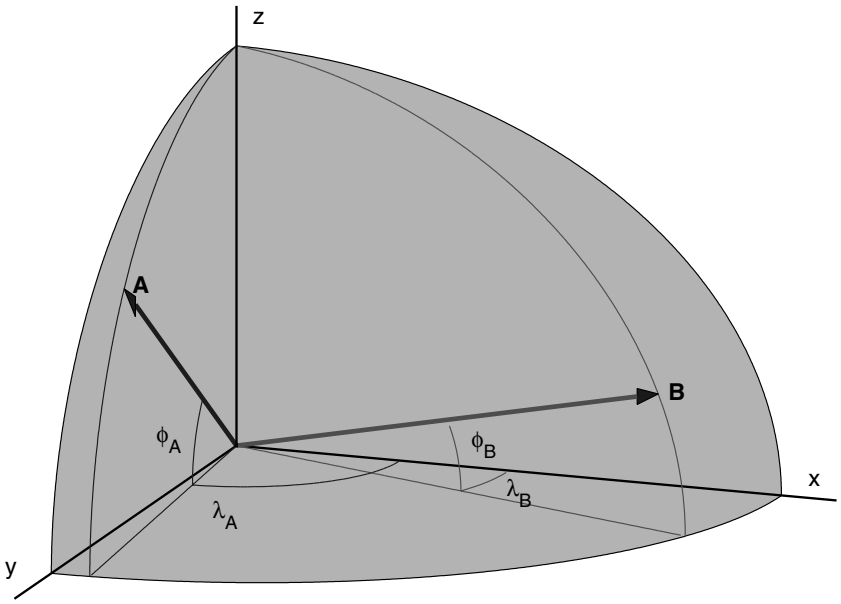

Figure 2. Illustrations of two unit vectors on the sphere, which are mathematically described completely by (λ_A, ϕ_A) and (λ_B, ϕ_B), respectively.

obtain two sets of (8) or equivalently (12). The erroneous set will be automatically eliminated in the process of inversion by using a robust estimation method, as in the case of automatically choosing the true fault plane from the two nodal planes of an earthquake focal mechanism for the determination of stress tensors (see e.g. Gephart & Forsyth 1984). Thus, for the correct sense of slip, we again automatically obtain two non-linear independent constraints of equality.

Since both slip directions and fault planes contain random errors, Angelier *et al.* (1982) first recast the model of stress tensor inversion from fault-slip data as a least-squares problem with non-linear constraints on the fault-slip parameters and the reduced stress tensor, and then estimated all the parameters and the tensor simultaneously. Although each fault-slip datum and the reduced tensor must satisfy two independent constraints, as explicitly represented by (12), Angelier *et al.* (1982) actually reformulated (6) or (8) as:

$$\|\mathbf{s} - \mathbf{f}_{\rm sn}\|^2 = 0, \tag{13a}$$

and obtained an equivalent new constraint,

$$\mathbf{s}^{\rm T}\boldsymbol{D}\mathbf{n} = \|\boldsymbol{D}\mathbf{n} - (\mathbf{n}^{\rm T}\boldsymbol{D}\mathbf{n})\mathbf{n}\|, \tag{13b}$$

which is formula (5) of Angelier *et al.* (1982). From a programming point of view, (8), (12) and (13b) are all equivalent mathematically. Thus Angelier *et al.* (1982) successfully used (13b) to simultaneously estimate the reduced stress tensor and were able to correct the fault planes and slip directions. However, from a statistical point of view, the linearization of (13b), or equivalently (13a), cannot be directly used to compute the accuracy of the stress parameters. The correct method for accuracy computation must be based on two functionally independent constraints of type (12). The proof of this conclusion is rather straightforward and is thus omitted here.

Unlike Angelier *et al.* (1982), McKenzie (1969) and Gephart & Forsyth (1984) only used the parallel condition of maximum shear stress and slip directions. Since that condition is not equivalent to the equality of $\mathbf{s}$ and $\mathbf{f}_{\rm sn}$ mathematically, one independent constraint has been missing in the work of Gephart & Forsyth (1984). Strictly speaking, the method of Gephart & Forsyth (1984) is not a technique for simultaneously estimating the stress tensor and fault-slip corrections (see also Liang & Wyss 1991; Gillard & Wyss 1995; Lu *et al.* 1997).

3 SOLUTIONS OF THE INVERSE PROBLEM

The inverse problem of determining stress tensors from fault-slip data has generally been solved in one of two ways: (i) treat both fault-slips and the reduced stress tensor as the unknown model parameters, and then solve them from the fault-slip data (see e.g. Angelier *et al.* 1982; Gephart & Forsyth 1984; Gephart 1990; Will & Powell 1991); but more often, (ii) treat fault planes as if they were free of random errors, and then determine the reduced tensor. Numerically, the inverse problem has been solved using iterative and/or grid search methods. Iterative methods are local optimization techniques and thus generally are not able to correctly find the global optimal stress tensor that best fits the cost function. Practical implementation of the grid search method does not correctly find the global optimal tensor either, as mentioned in Gephart & Forsyth (1984), since gridding cannot be made arbitrarily fine. If both types of method correctly find the optimal stress tensors, the difference in solutions may be small. However, the error estimate can be significantly different by one order of magnitude, as will be seen in Section 5. In this section, we will first give an alternative formulation of Angelier *et al.* (1982), and then propose using the global optimization method described in Appendix A to determine the global optimal reduced stress tensor.

3.1 Simultaneous determination of fault planes, slips and the tensor

Given n fault-slip measurements, namely, ϕ_i, δ_i, λ_i ($i = 1, 2, \ldots, n$), and denoting the corresponding *true* unknown fault plane angles and the slip angle by $\underline{\phi}_i, \underline{\delta}_i, \underline{\lambda}_i (i = 1, 2, \ldots, n)$, then we have, for each fault-slip datum, the following observation equations:

$$\phi_i = \underline{\phi}_i + \epsilon_{\phi_i}, \tag{14a}$$

$$\delta_i = \underline{\delta}_i + \epsilon_{\delta_i}, \tag{14b}$$

$$\lambda_i = \underline{\lambda}_i + \epsilon_{\lambda_i}, \tag{14c}$$

and two functionally independent constraints on $\underline{\phi}_i, \underline{\delta}_i, \underline{\lambda}_i$ and the reduced stress tensor $\boldsymbol{D}$:

$$g_{1i}(\underline{\phi}_i, \underline{\delta}_i, \underline{\lambda}_i, \boldsymbol{D}) = 0, \tag{15a}$$

$$g_{2i}(\underline{\phi}_i, \underline{\delta}_i, \underline{\lambda}_i, \boldsymbol{D}) = 0. \tag{15b}$$

Here g_{1i} and g_{2i} can be derived from and are mathematically equivalent to (8) or $\mathbf{s}_i = \mathbf{f}^i_{\rm sn}$ for the ith fault plane. $\epsilon_{\phi_i}, \epsilon_{\delta_i}$ and ϵ_{λ_i} are the random errors of ϕ_i, δ_i and λ_i, statistically independent and with zero means and variances $\sigma^2_{\phi i}, \sigma^2_{\delta i}$ and $\sigma^2_{\lambda i}$, respectively.

We introduce the following notation:

$$\mathbf{y}_i = (\phi_i, \delta_i, \lambda_i)^{\rm T}, \tag{16a}$$

$$\mathbf{V}_i = \mathrm{diag}\left(\sigma^2_{\phi_i}, \sigma^2_{\delta_i}, \sigma^2_{\lambda_i}\right), \tag{16b}$$

$$\mathbf{p}_i = (\underline{\phi}_i, \underline{\delta}_i, \underline{\lambda}_i)^{\rm T}, \tag{16c}$$

$$\mathbf{g}_i = \{g_{1i}(\underline{\phi}_i, \underline{\delta}_i, \underline{\lambda}_i, \boldsymbol{D}), g_{2i}(\underline{\phi}_i, \underline{\delta}_i, \underline{\lambda}_i, \boldsymbol{D})\}^{\rm T}. \tag{16d}$$

We collect the four tensor parameters of $\boldsymbol{D}$ in the following vector

$$\mathbf{d} = (\varphi, \alpha, \beta, \gamma)^{\rm T}, \tag{16e}$$

and denote the derivative matrices by

$$\mathbf{A}^k_i = \begin{bmatrix} \dfrac{\partial g_{1i}}{\partial \underline{\phi}_i} & \dfrac{\partial g_{1i}}{\partial \underline{\delta}_i} & \dfrac{\partial g_{1i}}{\partial \underline{\lambda}_i} \\ \dfrac{\partial g_{2i}}{\partial \underline{\phi}_i} & \dfrac{\partial g_{2i}}{\partial \underline{\delta}_i} & \dfrac{\partial g_{2i}}{\partial \underline{\lambda}_i} \end{bmatrix}, \tag{16f}$$

$$\mathbf{B}^k_i = \begin{bmatrix} \dfrac{\partial g_{1i}}{\partial \varphi} & \dfrac{\partial g_{1i}}{\partial \alpha} & \dfrac{\partial g_{1i}}{\partial \beta} & \dfrac{\partial g_{1i}}{\partial \gamma} \\ \dfrac{\partial g_{2i}}{\partial \varphi} & \dfrac{\partial g_{2i}}{\partial \alpha} & \dfrac{\partial g_{2i}}{\partial \beta} & \dfrac{\partial g_{2i}}{\partial \gamma} \end{bmatrix}, \tag{16g}$$

where k stands for the kth iteration, and $\mathbf{A}^k_i$ and $\mathbf{B}^k_i$ are computed at points $\mathbf{p}^k_i$ and $\mathbf{d}^k$.

In order to estimate $\mathbf{p}_i$ ($i = 1, 2, \ldots, n$) and $\mathbf{d}$ simultaneously, we collect all the fault-slip data of (14) and the constraints of (15) together. The inverse problem can now be formulated as follows:

$$\min: \sum_{i=1}^{n} \left\{ \frac{(\phi_i - \underline{\phi}_i)^2}{\sigma^2_{\phi_i}} + \frac{(\delta_i - \underline{\delta}_i)^2}{\sigma^2_{\delta_i}} + \frac{(\lambda_i - \underline{\lambda}_i)^2}{\sigma^2_{\lambda_i}} \right\} \tag{17}$$

subject to $2n$ non-linear constraints of equality (15). Applying the solution technique of Britt & Luecke (1973) and Seber & Wild (1989), we ultimately obtain the iterative formulae:

$$\mathbf{d}^{k+1} = \mathbf{d}^k + \mathbf{N}_k^{-1} \sum_{i=1}^{n} \left(\mathbf{B}_i^k\right)^{\mathrm{T}} \left\{\mathbf{A}_i^k \mathbf{V}_i \left(\mathbf{A}_i^k\right)^{\mathrm{T}}\right\}^{-1} \times \left\{\mathbf{g}_i^k + \mathbf{A}_i^k \left(\mathbf{y}_i - \mathbf{p}_i^k\right)\right\}, \tag{18a}$$

with which to estimate the reduced stress tensor, and

$$\mathbf{p}_i^{k+1} = \mathbf{y}_i - \mathbf{V}_i \left(\mathbf{A}_i^k\right)^{\mathrm{T}} \left\{\mathbf{A}_i^k \mathbf{V}_i \left(\mathbf{A}_i^k\right)^{\mathrm{T}}\right\}^{-1} \times \left\{\mathbf{g}_i^k + \mathbf{A}_i^k \left(\mathbf{y}_i - \mathbf{p}_i^k\right) + \mathbf{B}_i^k (\mathbf{d}^{k+1} - \mathbf{d}^k)\right\}, \tag{18b}$$

($i = 1, 2, \ldots, n$), with which to correct the fault-slip parameters for each fault plane, where

$$\mathbf{N}_k = \sum_{i=1}^{n} \left(\mathbf{B}_i^k\right)^{\mathrm{T}} \left\{\mathbf{A}_i^k \mathbf{V}_i \left(\mathbf{A}_i^k\right)^{\mathrm{T}}\right\}^{-1} \mathbf{B}_i^k.$$

Eqs (18) are the mathematically correct solution to the constrained least-squares problem (17). However, it is only locally optimal, since there exists no guarantee that it converges to the global optimal solution of (17) subject to the constraints of equality. It is much simpler than equation (18) of Angelier *et al.* (1982), because we need only invert n (2×2) matrices to compute $\mathbf{p}_i^{k+1}$($i = 1, 2, \ldots, n$) of (18b) and a (4×4) matrix to compute $\mathbf{d}^{k+1}$ of (18a) at each iteration, whereas Angelier *et al.* (1982) needed to solve for all the fault-slip parameters and the reduced stress tensor by inverting a matrix of dimension ($n + 4$). Thus our alternative formulation is computationally more effective. More importantly, after the solution has been found, our formulation can be directly used to compute the accuracy of the solution. From a statistical point of view, the formulae given by Angelier *et al.* (1982) cannot be used to compute the accuracy of the solution, as will be confirmed in Section 5.

3.2 Determination of the reduced tensor with fixed fault-slip parameters

In the second common approach to stress tensor inversion, most researchers fix fault planes and slip angles as if they were free of errors, and then focus on the determination of the four parameters that describe the reduced stress tensor. A major limitation of this practice is that the errors in the fault planes are not used in statistical assessment of the resultant stress tensor. Fixing the fault planes as if they were free of errors is equivalent to applying no corrections to the fault plane and slip parameters. Thus the starting equation (8) has been effectively turned into observation equations. Since fault planes and slips are never error-free, (8) cannot be exact. Nevertheless, the majority of research is focused on establishing optimal criteria with which to estimate the reduced stress tensor from fault-slip data. A number of such criteria have been proposed, either with or without prior information about the stress tensor (see e.g. Carey & Brunier 1974; Armijo & Cisternas 1978; Angelier 1979, 1990; Etchecopar *et al.* 1981; Angelier *et al.* 1982; Gephart & Forsyth 1984; Will & Powell 1991; Yin & Ranalli 1993).

Suppose that an optimal criterion has been described by a proper positive scalar function ρ to measure the difference between the left- and right-hand sides of (8). Then estimating the reduced stress tensor is equivalent to solving the following unconstrained minimization problem:

$$\min: \sum_{i=1}^{n} \rho\left(\mathbf{s}_i, \left\{\boldsymbol{D}\mathbf{n}_i - \left(\mathbf{n}_i^{\mathrm{T}} \boldsymbol{D}\mathbf{n}_i\right)\mathbf{n}_i\right\} \Big/ \left\|\boldsymbol{D}\mathbf{n}_i - \left(\mathbf{n}_i^{\mathrm{T}} \boldsymbol{D}\mathbf{n}_i\right)\mathbf{n}_i\right\|\right) \tag{19}$$

where i is the index of the ith fault plane and, the positive scalar function $\rho(x)$ is a weighted L_1-norm, weighted L_2-norm, $\cos^2 x$, or other similar functions.

To date, none of the solutions to (19) in the literature on stress tensor inversion are guaranteed to produce the global optimal reduced tensor. We will use the new global optimization method described in Appendix A to solve (19). The advantage of using the new method is that we can always correctly find the global optimal reduced tensor(s). In this paper, we will use the L_2-norm to estimate **d** of (16e). If fault-slip data are of different accuracy, then a weight matrix describing the different importance of different fault-slip data should be used. For this particular cost function, we will use the damped least-squares (Gauss–Newton) method to find the local optimal solution in the neighbourhood of a given feasible point, because it is locally convergent for almost all non-linear least-squares problems (Dennis & Schnabel 1996). The algorithm of the damped least-squares method is given as follows:

$$\mathbf{d}^{k+1} = \mathbf{d}^k - \mu_k \left\{\sum_{i=1}^{n} \left(\mathbf{B}_i^k\right)^{\mathrm{T}} \mathbf{B}_i^k\right\}^{-1} \sum_{i=1}^{n} \left(\mathbf{B}_i^k\right)^{\mathrm{T}} \mathbf{g}_i^k, \tag{20}$$

where k is the iterate index, the positive scalar μ_k is obtained by a line search, and the three components of $\mathbf{g}_i^k$ are defined as follows:

$$g_{1i}\left(\phi_i, \delta_i, \lambda_i, \mathbf{d}^k\right) = f_{\mathrm{ns}}^{1i}\left(\phi_i, \delta_i, \mathbf{d}^k\right) - s_{1i}(\phi_i, \delta_i, \lambda_i)$$

$$g_{2i}\left(\phi_i, \delta_i, \lambda_i, \mathbf{d}^k\right) = f_{\mathrm{ns}}^{2i}\left(\phi_i, \delta_i, \mathbf{d}^k\right) - s_{2i}(\phi_i, \delta_i, \lambda_i)$$

$$g_{3i}\left(\phi_i, \delta_i, \lambda_i, \mathbf{d}^k\right) = f_{\mathrm{ns}}^{3i}\left(\phi_i, \delta_i, \mathbf{d}^k\right) - s_{3i}(\phi_i, \delta_i, \lambda_i),$$

for each fault-slip datum. $f_{\mathrm{ns}}^{1i}, f_{\mathrm{ns}}^{2i}$ and f_{ns}^{3i} are three components of the unit vector $\mathbf{f}_{\mathrm{ns}}$. The matrix $\mathbf{B}_i^k$ is given by

$$\mathbf{B}_i^k = \begin{bmatrix} \frac{\partial g_{1i}}{\partial \varphi} & \frac{\partial g_{1i}}{\partial \alpha} & \frac{\partial g_{1i}}{\partial \beta} & \frac{\partial g_{1i}}{\partial \gamma} \\ \frac{\partial g_{2i}}{\partial \varphi} & \frac{\partial g_{2i}}{\partial \alpha} & \frac{\partial g_{2i}}{\partial \beta} & \frac{\partial g_{2i}}{\partial \gamma} \\ \frac{\partial g_{3i}}{\partial \varphi} & \frac{\partial g_{3i}}{\partial \alpha} & \frac{\partial g_{3i}}{\partial \beta} & \frac{\partial g_{3i}}{\partial \gamma} \end{bmatrix}.$$

Alternatively, one may also use the Levenberg–Marquardt algorithm:

$$\mathbf{d}^{k+1} = \mathbf{d}^k - \left\{\sum_{i=1}^{n} \left(\mathbf{B}_i^k\right)^{\mathrm{T}} \mathbf{B}_i^k + \mu_k \mathbf{I}\right\}^{-1} \sum_{i=1}^{n} \left(\mathbf{B}_i^k\right)^{\mathrm{T}} \mathbf{g}_i^k, \tag{21}$$

to find a local optimal solution. Here μ_k is positive and can be chosen by using a number of strategies (see e.g. Dennis & Schnabel 1996).

As one of the components of our global optimization algorithm (Appendix A), we implement the damped least-squares method (20) as a local optimizer. Unlike the gridding method of Gephart & Forsyth (1984), our algorithm will automatically detect the degeneracy of the system, since the geometry of faults/striae has been fully taken into account. As a result, outputting a degenerate solution as the optimal stress tensor is avoided.

Eq. (19) can also be reformulated as a simultaneous estimation problem. In order to do so, we first fix any two of (ϕ_i, δ_i, λ_i) and leave the remaining one as an unknown parameter to be estimated in (19). We can then eliminate the two functionally independent non-linear constraints of equalities (15) by representing $\underline{\phi}_i$ and $\underline{\delta}_i$ with $\underline{\lambda}_i$ and the four tensor parameters, say, symbolically,

$$\underline{\phi}_i = h_{i1}(\underline{\lambda}_i, \varphi, \alpha, \beta, \gamma), \tag{22a}$$

$$\underline{\delta}_i = h_{i2}(\underline{\lambda}_i, \varphi, \alpha, \beta, \gamma). \tag{22b}$$

By inserting (22) into (17), we finally obtain a new least-squares problem of type (19) without constraints of any kind for simultaneously estimating **d** and fault-slip corrections.

4 THE EFFECT OF NON-LINEARITY ON INVERTED STRESS TENSORS

In this section, we analyse the statistical measures of bias and accuracy of the estimated global optimal tensor. Because most stress tensor inversions are concerned with estimating the four stress parameters **d** from fault-slip data by minimizing (19), we will use the L_2-norm in (19) and focus on the bias and accuracy analysis of the reduced stress tensor. Here we follow the second common approach and thus apply no corrections to the fault-slip data. However, we will fully take all the errors in the fault planes and slips into consideration for the computation of biases and accuracy. In what follows, we assume that the fault-slip data are stochastically independent from one fault to another, namely,

$$E(\boldsymbol{\epsilon}_i) = \mathbf{0}, \tag{23a}$$

$$E\left(\boldsymbol{\epsilon}_i \boldsymbol{\epsilon}_i^{\mathrm{T}}\right) = \mathbf{V}_i, \tag{23b}$$

for all i, and

$$E\left(\boldsymbol{\epsilon}_i \boldsymbol{\epsilon}_j^{\mathrm{T}}\right) = \mathbf{0}, \tag{23c}$$

if $i \neq j$. Here $\boldsymbol{\epsilon}_i = (\epsilon_{\phi_i}, \epsilon_{\delta_i}, \epsilon_{\lambda_i})^{\mathrm{T}}$, $\mathbf{V}_i$ is a (positive-definite) variance-covariance matrix of $\boldsymbol{\epsilon}_i$. Given a scalar function $f_i(\mathbf{x}, \mathbf{y})$ and a vector function $\mathbf{f}(\mathbf{x})$, we denote the matrix of second-order partial derivatives of $f_i(\mathbf{x}, \mathbf{y})$ with respect to $\mathbf{x}$ and $\mathbf{y}$ by

$$\ddot{\mathbf{f}}_{ixy} = \left[\frac{\partial^2 f_i(\mathbf{x}, \mathbf{y})}{\partial \mathbf{x} \partial \mathbf{y}^{\mathrm{T}}}\right],$$

and the matrix of first-order partial derivatives of $\mathbf{f}(\mathbf{x})$ with respect to $\mathbf{x}$ by

$$\dot{\mathbf{f}}_x = \left[\frac{\partial \mathbf{f}(\mathbf{x})}{\partial \mathbf{x}^{\mathrm{T}}}\right].$$

The derivatives higher than the second order will be neglected in the computation of biases and accuracy. For brevity, we will replace the unit vector $\mathbf{f}_{\mathrm{sn}}$ with $\mathbf{f}$, and assign a subscript i to $\mathbf{f}$ or $\mathbf{s}$ to stand for the ith fault-slip data.

4.1 Biases of the parameters of the inverted stress tensor

Denote the estimated and true but unknown stress tensor parameters by $\hat{\mathbf{d}}$ and $\mathbf{d}$, respectively, and denote the biases of $\hat{\mathbf{d}}$ by $\mathbf{b}(\hat{\mathbf{d}})$. Then by definition, $\mathbf{b}(\hat{\mathbf{d}})$ is computed as follows:

$$\mathbf{b}(\hat{\mathbf{d}}) = E(\hat{\mathbf{d}} - \mathbf{d}), \tag{24}$$

where $E()$ stands for the expectation operator. If the L_2-norm is used to solve (19), we obtain

$$\mathbf{b}(\hat{\mathbf{d}}) = \left(\sum_{i=1}^{n} \dot{\mathbf{f}}_{id}^{\mathrm{T}} \dot{\mathbf{f}}_{id}\right)^{-1} (\mathbf{b}_s + \mathbf{b}_{f_\epsilon} + \mathbf{b}_{f_d} + \mathbf{b}_{f_{\epsilon d}}) \tag{25}$$

after a lengthy derivation, where $\mathbf{b}_s$, $\mathbf{b}_{f_\epsilon}$, $\mathbf{b}_{f_d}$ and $\mathbf{b}_{f_{\epsilon d}}$ are all given in Appendix B.

It is obvious from (25) (also compare Appendix B) that the contribution to the biases of the inverted stress tensor parameters is fourfold: (i) the non-linearity of the unit slip vector $\mathbf{s}_i$ with respect to the fault-slip errors; (ii) the non-linearity of the resolved maximum shear with respect to the fault-slip errors; (iii) the non-linearity of the resolved maximum shear with respect to the four stress tensor parameters; and (iv) the combined non-linearity of the resolved maximum shear with respect to the stress parameters and the fault plane errors. These results are quite interesting, since they indicate that the linear inversion for stress tensors from fault planes and slip directions, together with prior assumptions on the magnitudes of shears (Michael 1984) or empirical relationships of the three principal stresses (Angelier 1989), is also biased. In this case, although the inversion is linear with respect to the stress tensor parameters, only (40d), namely the bias term involved with the second derivatives of the resolved maximum shear with respect to the stress parameters, will disappear from (25). The non-linearity of fault-slip data will still bias the estimated stress tensor obtained with linear inversion. By slightly modifying the results of Xu & Grafarend (1996), we can compute the biases of the principal stress directions and the shape parameter of the inverted stress ellipsoid, which will also be shown in Section 5.

4.2 Accuracy of the inverted stress tensor

Although exact computation of the variance–covariance matrix of $\hat{\mathbf{d}}$ is complicated, one can easily obtain its first-order approximation. Actually, by discarding the second-order term $\mathbf{q}$ from (36) and then applying the error propagation law to the linear approximation, we obtain

$$\Sigma_{\hat{\mathbf{d}}}^{1} = \mathbf{H}\mathbf{V}\mathbf{H}^{\mathrm{T}} = \sum_{i=1}^{n} \mathbf{H}_i \mathbf{V}_i \mathbf{H}_i^{\mathrm{T}}, \tag{26}$$

where $\Sigma_{\hat{\mathbf{d}}}^{1}$ is the first-order approximation to the variance-covariance matrix of $\hat{\mathbf{d}}$. If the errors in fault planes are not taken into account in the accuracy computation for $\hat{\mathbf{d}}$, then we will have to remove the terms of $\dot{\mathbf{f}}_{i\epsilon}$ from (26). Thus the linear approximation of accuracy without taking the errors of fault planes into account becomes:

$$\Sigma_{\hat{\mathbf{d}}}^{2} = \left(\sum_{i=1}^{n} \dot{\mathbf{f}}_{id}^{\mathrm{T}} \dot{\mathbf{f}}_{id}\right)^{-1} \left(\sum_{i=1}^{n} \dot{\mathbf{f}}_{id}^{\mathrm{T}} \dot{\mathbf{s}}_i \mathbf{V}_i \dot{\mathbf{s}}_i^{\mathrm{T}} \dot{\mathbf{f}}_{id}\right) \left(\sum_{i=1}^{n} \dot{\mathbf{f}}_{id}^{\mathrm{T}} \dot{\mathbf{f}}_{id}\right)^{-1}. \tag{27}$$

If the non-linearity of the model with respect to the fault-slip errors and stress parameters is severe and if the ratio of stress signal to stress noise is small, then the linear approximation (26) can be erroneous. In order to obtain a variance-covariance matrix of higher order, we will have to assume the moment information of higher order on fault-slip data accordingly. For instance, if we assume that $E(\epsilon_i \epsilon_j \epsilon_k) = 0$ for any i, j and k, and also assume that the fourth statistical moments of errors $E(\epsilon_i \epsilon_j \epsilon_k \epsilon_l)$ are all known, then we can compute the variance-covariance matrix of $\hat{\mathbf{d}}$ to second-order approximation, which is given by

$$\begin{aligned} \Sigma_{\hat{\mathbf{d}}} &= E\{[\mathbf{p} - E(\mathbf{p})][\mathbf{p} - E(\mathbf{p})]^{\mathrm{T}}\} \\ &= \sum_{i=1}^{n} \mathbf{H}_i \mathbf{V}_i \mathbf{H}_i^{\mathrm{T}} + E(\mathbf{q}\mathbf{q}^{\mathrm{T}}) - \mathbf{b}(\hat{\mathbf{d}})\mathbf{b}^{\mathrm{T}}(\hat{\mathbf{d}}). \end{aligned} \tag{28}$$

If the derivatives higher than second order are negligible, then (28) is sufficiently accurate. Since $E(\mathbf{q}\mathbf{q}^{\mathrm{T}}) - \mathbf{b}(\hat{\mathbf{d}})\mathbf{b}^{\mathrm{T}}(\hat{\mathbf{d}}) \geq \mathbf{0}$, the first-order approximation will often overestimate the accuracy of the inverted stress tensor from fault-slip data.

5 FAULT-SLIP DATA AND RESULTS

The fault-slip data in this paper are taken from Angelier *et al.* (1982). This data set consists of 33 fault orientations measured at Agia Varvara, central Crete. All the faults are normal. Since three of the fault-slip data were found to be anomalously inconsistent with the other 30 faults, they will be excluded from this investigation, as they were by Angelier *et al.* (1982). The measured values (ϕ_i, δ_i, λ_i) for

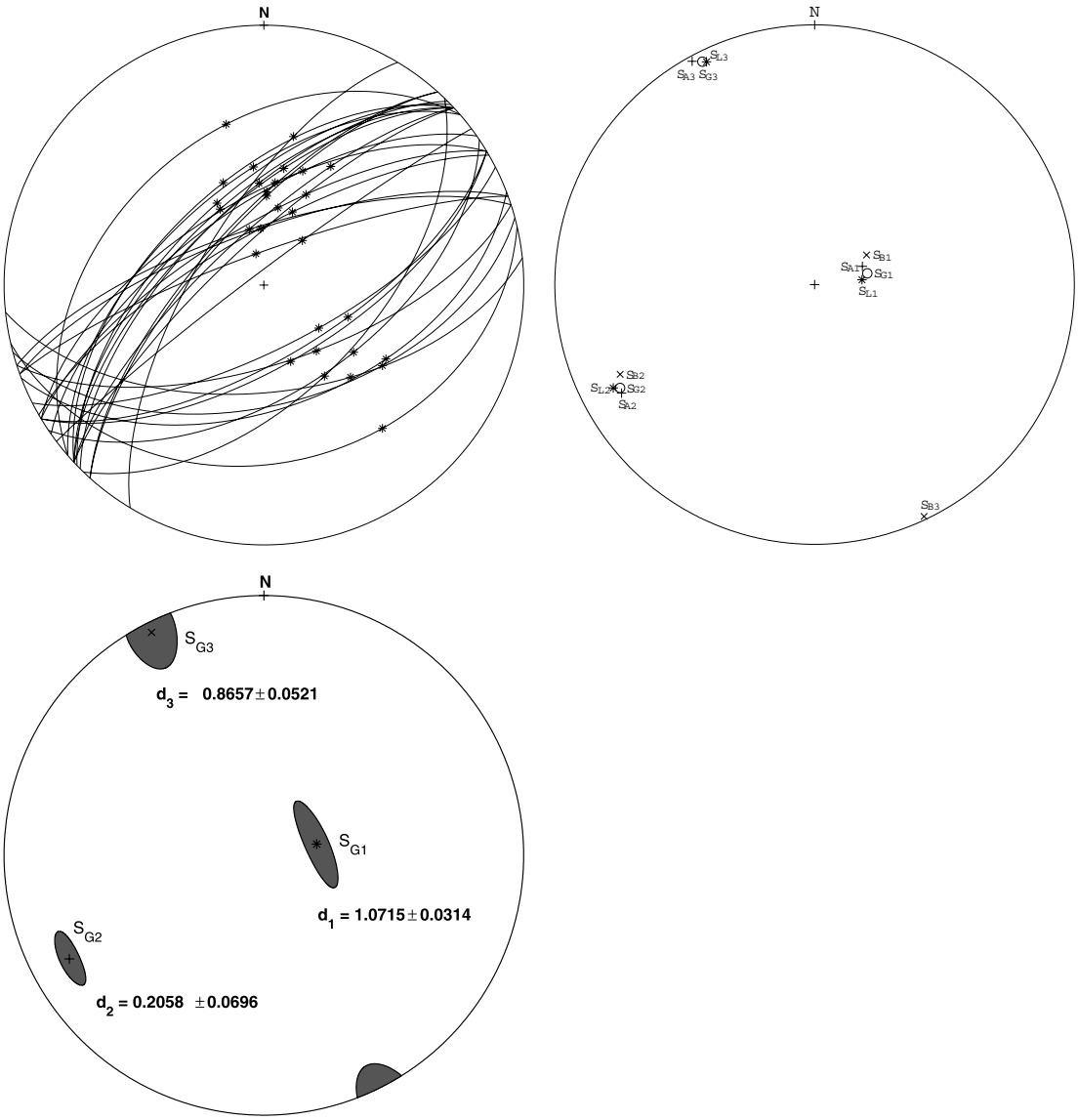

Figure 3. Fault-slip data and directions of the principal stresses. Top-left plot: Lower hemisphere projections of fault planes and slip data. The slip vectors of the hanging blocks relative to the footwall blocks are shown with stars and all radiate from the centre of the circle. Top-right plot: Lower hemisphere projections of the directions of the principal stresses. Only four of the five stress tensors listed in Table 2 are shown here, namely, *Linear*, *Constrained*, *Global* and *Bias-corrected*, which are marked with $*$, $+$, o and $\times$, and are assigned the first subscript indices L, A, G and B, respectively. The second subscript indices are arranged from most compressive to least compressive (or tensile). Bottom plot: The principal stresses and their accuracy, and the 99 per cent probability confidence ellipses (shaded areas) of the principal eigendirections of the global optimal stress tensor.

all the retained faults are presumed to be statistically independent and of the same accuracy of 7°. Since our coordinate system and definition of fault-slip data are slightly different from those used by Angelier *et al.* (1982), we have transformed the data used in our computation. However, in order to compare our results with those of Angelier *et al.* (1982), we will have to give all the tensors and tensor parameters in the rest of this paper by using the second sign tensor convention. The data set with the three problematic faults removed is shown in Fig. 3. For more details on the data, the reader is referred to Angelier *et al.* (1982).

In order to apply the new hybrid global optimization method to finding the global optimal stress tensor(s), we assume that no prior information is available on the four stress parameters **d**. Since the smallest domain of definition for φ is between 0 and 2π, the initial box for φ is naturally chosen to be $[0, 2\pi]$. For the other three stress parameters α, β and γ, in order not to miss the optimal stress tensor(s), we have to use the largest possible initial bounding box for them. More specifically, α, β and γ are all supposed to be within $[-10^8, 10^8]$. The convergence criteria of the damped least squares are set to be $|\delta x_i| < 10^{-8}$, where x_i is any one of the four stress parameters φ, α, β or γ. Test computation has shown that there exist many local solutions in the small neighbourhood of the global optimal solution. In order not to spend too much time searching for negligibly different solutions within a very small box, we will stop searching if any side of the box under investigation is smaller than 0.001.

Although a starting point does not affect our method to find correctly the global optimal stress tensor(s) (see e.g. Xu 2002, 2003a), it may influence the convergence speed. Generally, one may randomly sample a number of points and then choose the best one from

Table 1. The four stress parameters from linear inversion, simultaneous inversion of fault-slips and stress tensors, the first local inversion and the global inversion.

Methods	φ	α	β	γ	Cost
Linear	2.415	0.306	−0.318	0.033	0.685063
Constrained	2.471	0.481	−0.260	−0.055	0.962133
Local	2.361	0.270	−0.323	−0.023	0.651680
Global	2.381	0.286	−0.371	−0.030	0.633044

Table 2. The shape parameters of stress ellipsoids and the principal orientations (in degrees) of four stress tensors with the stress parameters in Table 1. The principal directions of stress are arranged from most compressive to least compressive (or tensile).

Tensors	Shapes	1st principal axis		2nd principal axis		3rd principal axis	
		Azimuth	Plunge	Azimuth	Plunge	Azimuth	Plunge
Linear	0.60	84.24	75.10	242.84	13.91	334.14	5.23
Constrained	0.47	69.07	73.98	240.64	15.86	331.27	2.23
Local	0.66	78.48	75.20	242.49	14.25	333.49	3.91
Global	0.66	77.90	73.07	241.98	16.32	333.27	4.40
Bias-corrected	0.70	60.31	71.24	245.21	18.70	154.71	1.49

which to start our global optimization method. We would prefer to use a theoretically sound method to find a starting point, if it is not computationally costly and if it is believed to be capable of producing a reasonably good starting point. In this paper, however, we will use the linear inversion of Michael (1984) by constraining the magnitudes of shears on all the faults to find the starting stress tensor, which is given, after being rescaled to the stress tensor of four parameters, as follows:

$$\begin{bmatrix} -0.7477 & 0.3061 & 0.0335 \\ 0.3061 & -0.2013 & -0.3184 \\ 0.0335 & -0.3184 & 0.9489 \end{bmatrix}.$$

The four stress parameters from the global stress inversion are listed in the last row (*Global*) of Table 1. For convenience, we have also listed in Table 1 the results obtained with the linear inversion of Michael (1984) (*Linear*), the results taken from Angelier *et al.* (1982) (*Constrained*), and the results from the first iteration of our global optimal inversion (*Local*). The cost values (19) of these four stress tensors are given in Table 1 as well. Since the coordinate system used in Angelier *et al.* (1982) is different from ours, the results of Angelier *et al.* (1982) have to be correspondingly transformed into our system for convenience of comparison. The global inversion results are in good agreement with those of Angelier *et al.* (1982) and those from the linear inversion of Michael (1984). We have also tested some other different starting points; some of these local solutions, (6.283, 8.336, −3.989, 1.567) with the cost value of 22.006, for example, can be far away from the global optimal tensor, however. Table 2 lists the three principal orientations and the shape parameter for each of the four stress ellipsoids with the stress parameters in Table 1, and the stress ellipsoid with the bias-corrected stress parameters. The orientations of the three principal stresses for each of the tensors in Table 2 except *Local* are also shown in Fig. 3. All the five stress tensors are very close to each other in terms of the three principal orientations and the shape parameter, except for the azimuthal component of the third axis of the bias-corrected tensor.

We may note from the point of view of invariance that $\boldsymbol{D}$ cannot be distinguished from the whole class of tensors $\boldsymbol{T}(=t_s\boldsymbol{D} + t_v\mathbf{I})$. This implies mathematically that the first and third principal stress directions of $\boldsymbol{D}$ could correspond, respectively, to the third and first principal stress directions of $\boldsymbol{T}$, although the second (intermediate) principal stress direction remains unchanged. For this specific set of data, since we know the type of fault, we can correctly conclude that the reduced stress tensor matches the normal faults exactly. For practical applications, if the type of fault is known without ambiguity, as in the above example, it is trivial to correctly identify the reduced stress tensor that matches the data. In the case of earthquake focal mechanism data, since we have no prior knowledge about the type of faulting before computation, we suggest a practical guide in order to check or confirm the correct reduced stress tensor $\boldsymbol{D}$. As a first step, one simply computes the (ambiguous) reduced stress tensor by using a robust version of the method described in this paper. Secondly, substitute the estimated $\boldsymbol{D}$ back into the focal mechanism data and eliminate the incorrect nodal planes from the focal mechanism data. And finally, use the remaining, unambiguous fault planes to decide the reduced stress tensor that matches the data, and continue for geophysical interpretations.

Table 3 lists the first-order accuracy of the four stress parameters, with and without taking fault plane errors into account. If the uncertainties in fault planes are not taken into account, the estimated accuracy is too optimistic by a factor of 4 to 9. Using the variance–covariance matrix of the global optimal stress tensor, we

Table 3. The accuracy of the four stress parameters with and without taking the errors of fault planes into account, respectively in the rows *Accuracy (error)* and *Accuracy (free)*, and their estimated biases $\mathbf{b}_{\hat{d}}$. The accuracy in the row *Accuracy (A1982)* is taken from Angelier *et al.* (1982) but has been transformed to our system for comparison.

Methods	φ	α	β	γ
Accuracy (error)	0.037	0.063	0.085	0.148
Accuracy (free)	0.009	0.007	0.011	0.022
Accuracy (A1982)	0.108	0.121	0.099	0.151
Biases $\mathbf{b}_{\hat{d}}$	0.030	0.002	−0.013	0.192

Table 4. The contribution of each source of non-linearity to the estimated biases $\mathbf{b}_{\hat{d}}$ of the four stress parameters: $\ddot{s}$, the non-linearity of slip directions w.r.t. ϕ, δ and λ; $\ddot{f}_\epsilon$, the non-linearity of the maximum shear directions w.r.t. ϕ, δ and λ; $\ddot{f}_d$, the non-linearity of the maximum shear directions w.r.t. the four stress parameters and $\ddot{f}_{\epsilon d}$, the combined non-linearity of the maximum shear directions w.r.t. ϕ, δ, λ and the four stress parameters.

Non-linearity	φ	α	β	γ
$\ddot{s}$	−0.003	−0.002	0.010	0.003
$\ddot{f}_\epsilon$	0.042	−0.013	−0.075	0.293
$\ddot{f}_d$	−0.059	0.013	0.074	−0.142
$\ddot{f}_{\epsilon d}$	0.050	0.003	−0.022	0.039

also compute the accuracy of the corresponding principal stresses, which are shown in the bottom plot of Fig. 3. Also shown in this part of the figure are the 99 per cent probability confidence ellipses for the three principal directions of the global optimal stress tensor. In conclusion, although fault planes could be treated as fixed in the stress inversion from fault-slip/focal mechanism data, their errors must be fully considered in order to obtain realistic accuracy for the resolved stress tensor. It is surprising that the accuracy of the four stress parameters given in Angelier *et al.* (1982) is generally worse than that obtained here with the errors of fault planes taken into account. Theoretically speaking, the simultaneous inversion should have produced a better measure of accuracy. This deviation of accuracy can be explained theoretically based on Section 3, since it has been found there that the formula in Angelier *et al.* (1982) does not compute the accuracy of the estimated quantities correctly from the statistical point of view. The biases of the four stress parameters are also listed in Table 3. Although they are generally quite small, the biases for φ and γ are equivalent to their respective uncertainties. In particular, note that the estimated values of α, β and γ are of the same order as the bias of the estimated $\hat{\gamma}$, however. This component of biases is even about six times larger than its estimated value numerically. In order to gain more insight into the effect of different sources of non-linearity, we have also computed the contribution of each type of non-linearity to the total biases $\mathbf{b}_{\hat{d}}$ and shown them in Table 4. It is obvious that the most significant source of biases comes from the non-linearity of the maximum shear with respect to ϕ, δ and λ, and has resulted in an even bigger bias of 0.293 for $\hat{\gamma}$ (compare the last row of Table 3 with the row labelled $\ddot{f}_\epsilon$ of Table 4). The effect of the non-linearity of the maximum shears with respect to the four stress parameters is also significant for this example. If empirical rules on rupture and friction are implemented, the inversion is known to be linear and the full stress tensor can be completely determined (Angelier 1989). In this case, the effect of $\ddot{f}_d$ will be eliminated. To further see how the biases of the four stress parameters affect the stress tensor, we have corrected the estimate of $\hat{\mathbf{d}}$ and shown the principal stress orientations and the shape parameter of the stress ellipsoid in Table 2 (the row *Bias-corrected*). As a consequence of the bias in the parameter $\hat{\gamma}$, the bias-corrected tensor is significantly different from the global optimal stress tensor in the azimuth of the first principal axis by about 20°.

6 CONCLUSIONS

The inverse problem of determining stress from fault-slip and/or earthquake focal mechanism data is non-linear, unless empirical rules on rupture and friction are employed. Solutions to this non-linear inverse problem have generally been either based on a local optimization algorithm or on grid search. The global optimal stress tensor can usually not be guaranteed by these methods. We have applied the global optimization method developed recently to finding the global optimal stress tensor from fault-slip data. The example has also shown that the constrained linear inversion solution is a very good starting point to find a better local solution which is close to the global optimal solution.

Confidence regions for the estimated stress tensor have been investigated in detail using the results of grid searches (Gephart & Forsyth 1984) or the bootstrap resampling approach (Michael 1987; Albarello 2000). However, the bias issue of the estimated stress tensor has not been addressed in the literature. We have shown that four types of non-linearity contribute to the biases of the four stress parameters: (i) the non-linearity of the unit slip vector $\mathbf{s}_i$ with respect to the fault-slip errors; (ii) the non-linearity of the resolved maximum shear with respect to the fault-slip errors; (iii) the non-linearity of the resolved maximum shear with respect to the four stress tensor parameters; and (iv) the combined non-linearity of the resolved maximum shear with respect to the stress parameters and the fault plane errors. The second and third types of non-linearity are found to be significant in the case study. The bias of $\hat{\gamma}$ is greater than the accuracy level and of the same magnitude as the three stress parameters α, β and γ. It is obvious that any linear inversion for stress from fault-slip data is biased as well, because only the third type of non-linearity will disappear. Although the stress tensor can be determined by fixing the fault planes and slip directions, their errors must be fully taken into account in the accuracy computation, otherwise the accuracy of the solution will be erroneous.

One of the basic assumptions for stress inversion is that the directions of maximum shear stress represent those of slips on a fault plane (Wallace 1951; Bott 1959). We have reformulated this assumption as two independent constraints of equality, and thus provided an alternative formulation to that of Angelier *et al.* (1982). Our formulation is computationally more effective and provides the correct way to compute the accuracy of the stress parameters. Since Gephart & Forsyth (1984), among others, only used the parallel condition, the method of Gephart & Forsyth (1984) may not be said to be a technique for simultaneously estimating the stress tensor and fault-slip corrections.

Finally, we note that the estimated reduced stress tensor may or may not match the type of fault correctly, since the parameters t_s and t_v in $\boldsymbol{T}$ are free. Given a set of fault-slip data without ambiguity, it is easy to identify the correct reduced stress tensor that matches the type of data. In the case of earthquake focal mechanism data, since we have no prior knowledge about the type of faulting before computation, we suggest the following practical guide in order to identify the correct reduced stress tensor $\boldsymbol{D}$: (i) compute the (ambiguous) reduced stress tensor by using a robust version of the method described in this paper; (ii) substitute the estimated $\boldsymbol{D}$ back into the focal mechanism data and eliminate the incorrect nodal planes from the focal mechanism data; and (iii) use the remaining, unambiguous fault planes to decide the reduced stress tensor that matches the data, and continue for geophysical interpretations.

ACKNOWLEDGMENTS

I thank Prof. J. Angelier and Dr J. Townend very much for their many constructive and insightful comments, which have helped improve the paper substantially and clarify a number of points. Additional thanks go to Prof. J. Angelier for sending me the preprint of his GJI 2002 paper prior to its publication. I would also like to thank the Editor for the suggestion to include the hybrid global optimization method as Appendix. A lengthy discussion with Dr J. Townend and the Editor also finally helped me to identify a code error in part of linear inversion, which is very much appreciated.

REFERENCES

Albarello, D., 2000. A resampling approach to test stress-field uniformity from fault data, *Geophys. J. Int.,* **140,** 535–542.

Amadei, B. & Stephansson, O., 1997. *Rock Stress and its Measurement,* Chapman & Hall, London.

Angelier, J., 1979. Determination of the mean principal directions of stresses for a given fault population, *Tectonophysics,* **56,** T17–T26.

Angelier, J., 1984. Tectonic analysis of fault slip data sets, *J. geophys. Res.,* **B89,** 5835–5848.

Angelier, J., 1989. From orientation to magnitudes in paleostress determination using fault slip data, *J. struct. Geol.,* **11,** 37–50.

Angelier, J., 1990. Inversion of field data in fault tectonics to obtain the regional stress—III. A new rapid direct inversion method by analytical means, *Geophys. J. Int.,* **103,** 363–376.

Angelier, J., 1994. Fault slip analysis and palaeostress reconstruction, in: *Continental Deformation*, pp. 53–100, ed. Hancock, P.L., Pergamon Press, Oxford.

Angelier, J., 2002. Inversion of earthquake focal mechanisms to obtain the seismotectonic stress IV—a new method free of choice among nodal planes, *Geophys. J. Int.,* **150,** 588–609.

Angelier, J. & Manoussis, S., 1980. Classification automatique et distinction des phases superposées en tectonique de faille, *C. R. Acad. Sci. Paris,* **D290,** 651–654.

Angelier, J., Tarantola, A., Valette, B. & Manoussis, S., 1982. Inversion of field data in fault tectonics to obtain the regional stress—I. Single phase fault populations: a new method of computing the stress tensor, *Geophys. J. R. astr. Soc.,* **69,** 607–621.

Armijo, R. & Cisternas, A., 1978. Un problème inverse en microtectonique cassante, *C.R. Acad. Sci. Paris,* **D287,** 595–598.

Bertsekas, D.P., 1982. *Constrained Optimization and Lagrange Multiplier Methods,* Academic Press, New York.

Bott, M.H.P., 1959. The mechanics of oblique slip faulting, *Geol. Mag.,* **96,** 109–117.

Box, M.J., 1971. Bias in nonlinear estimation (with discussions), *J.R. Statist. Soc.,* **B33,** 171–201.

Britt, H.I. & Luecke, R.H., 1973. The estimation of parameters in nonlinear implicit models, *Technometrics,* **15,** 233–247.

Carey, E. & Brunier, M.B., 1974. Analyse théorique et numérique d'um modèle mécanique élémentaire appliqué à l'étude d'une population de failles, *C. R. Acad. Sci.* Paris, **D279,** 891–894.

Choi, P.-Y., Angelier, J. & Souffaché, B., 1996. Distribution of angular misfits in fault-slip data, *J. struct. Geol.,* **18,** 1353–1367.

Daniel, J.W., 1973. Newton's method for nonlinear inequalities, *Numer. Math.,* **21,** 381–387.

Dennis, J.E. & Schnabel, R.B., 1996. *Numerical Methods for Unconstrained Optimization and Nonlinear Equations,* SIAM, Philadelphia.

Dennis, J.E., El-Alem, M. & Williamson, K., 1999. A trust-region approach to nonlinear systems of equalities and inequalities, *SIAM J. Optim.,* **9,** 291–315.

Dupin, J.-M., Sassi, W. & Angelier, J., 1993. Homogeneous stress hypothesis and actual fault slip: a distinct element analysis, *J. struct. Geol.,* **15,** 1033–1043.

Ellsworth, W.L. & Xu, Z.H., 1980. Determination of the stress tensor from focal mechanism data, *EOS, Trans. Am. geophys. Un.,* **61,** 1117.

Etchecopar, A., Vasseur, G. & Daignieres, M., 1981. An inverse problem in microtectonics for the determination of stress tensors from fault striation analysis, *J. struct. Geol.,* **3,** 51–65.

Fletcher, R., 1999. *Practical Methods of Optimization,* 2nd edn, Wiley, New York.

Fry, N., 1999. Striated faults: visual appreciation of their constraint on possible paleostress tensors, *J. struct. Geol.,* **21,** 7–21.

Gephart, J.W., 1990. Stress and the direction of slip on fault planes, *Tectonics,* **9,** 845–858.

Gephart, J.W. & Forsyth, D.W., 1984. An improved method for determining the regional stress tensor using earthquake focal mechanism data: application to the San Fernando earthquake sequence, *J. geophys. Res.,* **B89,** 9305–9320.

Gillard, D. & Wyss, M., 1995. Comparison of strain and stress tensor orientation: Application to Iran and southern California, *J. geophys. Res.,* **B100,** 22 197–22 213.

Hansen, E., 1992. *Global Optimization Using Interval Analysis*, Marcel Dekker, New York.

Hardebeck, J.L. & Hauksson, E., 1999. Role of fluids in faulting inferred from stress field signatures, *Science,* **285,** 236–239.

Horiuchi, S., Rocco, G. & Hasegawa, A., 1995. Discrimination of fault planes from auxiliary planes based on simultaneous determinations of stress tensor and a large number of fault plane solutions, *J. geophys. Res.,* **B100,** 8327–8338.

Huang, Q., 1988. Computer-based method to separate heterogeneous sets of fault-slip data into sub-sets, *J. struct. Geol.,* **10,** 297–299.

Koyama, J., 1997. *The Complex Faulting Process of Earthquakes,* Kluwer Academic, Dordrecht.

Lay, T. & Wallace, T.C., 1995. *Modern Global Seismology,* Academic Press, San Diego.

Liang, B. & Wyss, M., 1991. Estimates of orientations of stress and strain tensors based on fault-plane solutions in the epicentral area of the Great Hawaiian earthquake of 1868, *Bull. seism. Soc. Am.,* **81,** 2320–2334.

Lisle, R.J., 1992. New method of estimating regional stress orientations: applications to focal mechanism data of recent British earthquakes, *Geophys. J. Int.,* **110,** 276–282.

Lu, Z., Wyss, M. & Pulpan, H., 1997. Details of stress directions in the Alaska subduction zone from fault plane solutions, *J. geophys. Res.,* **B102,** 5385–5402.

McKenzie, D.P., 1969. The relation between fault plane solutions for earthquakes and the directions of the principal stresses, *Bull. seism. Soc. Am.,* **59,** 591–601.

Mandl, G., 2000. *Faulting in Brittle Rocks,* Springer, Berlin.

Michael, A.J., 1984. Determination of stress from slip data: faults and folds, *J. geophys. Res.,* **B89,** 11 517–11 526.

Michael, A.J., 1987. Use of focal mechanisms to determine stress: a control study, *J. geophys. Res.,* **B92,** 357–368.

Nieto-Samaniego, A.F. & Alaniz-Alvarez, S.A., 1997. Origin and tectonic interpretation of multiple fault patterns, *Tectonophysics,* **270,** 197–206.

Nocedal, J. & Wright, S.J., 1999. *Numerical Optimization,* Springer, New York.

Pollard, D.D., Saltzer, S.D. & Rubin, A.M., 1993. Stress inversion methods: are they based on faulty assumptions?, *J. struct. Geol.,* **15,** 1045–1054.

Polyak, B.T., 1964. Gradient methods for solving equations and inequalities, *USSR comput. Math. math. Phys.,* **4,** 17–32.

Pshenichnyi, B.N., 1970. Newton's method for the solution of systems of equalities and inequalities, *Math. Notes Acad. Sci. USSR,* **8,** 827–830.

Ramsay, J.G. & Lisle, R.J., 2000. *The Techniques of Modern Structural Geology,* Academic Press, San Diego.

Robinson, S.M., 1972. Extension of Newton's method to nonlinear functions with values in a cone, *Numer. Math.,* **19,** 341–347.

Seber, G. & Wild, C., 1989. *Nonlinear Regression,* John Wiley, New York.

Townend, J. & Zoback, M.D., 2001. Implications of earthquake focal mechanisms for the frictional strength of the San Andreas fault system, in: *The Nature and Tectonic Significance of Fault Zone Weakening,* pp. 13–21, eds Holdsworth, R.E., Strachan, R.A., Magloughlin, J.F. & Knipe, R.J., Geological Society of London, London.

Wallace, R.E., 1951. Geometry of shearing stress and relation to faulting, *J. Geol.,* **59,** 118–130.
Will, T.M. & Powell, R., 1991. A robust approach to the calculation of paleostress fields from fault plane data, *J. struct. Geol.,* **13,** 813–821.
Wyss, M. & Lu, Z., 1995. Plate boundary segmentation by stress directions: Southern San Andreas fault, California, *Geophys. Res. Lett.,* **22,** 547–550.
Xu, P.L., 1999. Spectral theory of constrained second-rank symmetric random tensors, *Geophys. J. Int.,* **138,** 1–24.
Xu, P.L., 2002. A hybrid global optimization method: the one-dimensional case, *J. comput. appl. Math.,* **147,** 301–314.
Xu, P.L., 2003a. A hybrid global optimization method: the multi-dimensional case, *J. comput. appl. Math.,* **155,** 423–446.
Xu, P.L., 2003b. Numerical solutions for bounding feasible point sets, *J. comput. appl. Math.,* **156,** 201–219.
Xu, P.L. & Grafarend, E., 1996. Statistics and geometry of the eigenspectra of 3-D second-rank symmetric random tensors, *Geophys. J. Int.,* **127,** 744–756.
Xu, Z., Wang, S., Huang, Y. & Gao, A., 1992. Tectonic stress field of China inferred from a large number of small earthquakes, *J. geophys. Res.,* **B97,** 11 867–11 877.
Yamaji, A., 2000. The multiple inverse method: a new technique to separate stresses from heterogeneous fault-slip data, *J. struct. Geol.,* **22,** 441–452.
Yin, Z.-M. & Ranalli, G., 1993. Determination of tectonic stress field from fault slip data: towards a probabilistic model, *J. geophys. Res.,* **B98,** 12 165–12 176.
Zoback, M.L., 1992. First- and second-order patterns of stress in the lithosphere: the World Stress Map project, *J. geophys. Res.,* **B97,** 11 703–11 728.

APPENDIX A: A HYBRID GLOBAL OPTIMIZATION METHOD

Inverse problems are generally non-linear and non-convex. Simulated annealing and genetic algorithms have most often been used in order to find the global optimal solutions to non-linear non-convex inverse problems in Earth Sciences. Since the algorithms of these types are of a random search nature, they are in practice not capable of correctly finding the global optimal solutions.

In this appendix we will briefly outline a hybrid global optimization method recently proposed by Xu (2002) in the 1-D case and then further extended by Xu (2003a,b) to the multidimensional case. The method consists of two basic components: local optimizers and feasible point finders. Local optimizers provide the efficiency and speed of finding a local optimal solution in the neighbourhood of a feasible point. Feasible point finders either guide the algorithm to produce a better local optimal solution or theoretically confirm that the local solution obtained at the previous step is globally optimal.

Consider the following non-linear non-convex optimization model:

$$\min: f(\mathbf{x}), \tag{29a}$$

subject to the constraint,

$$\mathbf{x} \in \mathbb{X}, \tag{29b}$$

where $f(\cdot)$ maps $\mathbb{X}$ into $\mathbb{Y}$, $\mathbb{X}$ is a subset of R^n and is either given explicitly or determined implicitly by some (linear or non-linear) constraints, and $\mathbb{Y} \in R$. Here we assume that $\mathbb{X}$ is a parallelepiped box. If the box $\mathbb{X}$ is sufficiently large, the minimization problem (29) becomes unconstrained.

By local optimizers, we mean any optimization algorithm that can produce a local optimal solution in the neighbourhood of a starting point. Optimization methods of local nature have been well developed and shown to be robust, reliable and fast in finding such a solution (e.g. Bertsekas 1982; Dennis & Schnabel 1996; Fletcher 1999; Nocedal & Wright 1999). A local optimizer can be formally represented by the following iteration procedure:

$$\mathbf{x}_{k+1} = \mathbf{x}_k + \alpha_k \mathbf{u}_k, \tag{30}$$

where k is the iteration index, α_k is a positive parameter that determines the length of a step for the next search from $\mathbf{x}_k$, and $\mathbf{u}_k$ is a unit vector that guides the direction of the next search. Local optimizers differ in the method of computing $\mathbf{u}_k$. As a consequence, the performance of local optimization methods can vary significantly, depending on whether $\mathbf{u}_k$ is determined with or without derivative information. In the Earth sciences, the simplex method and the damped least squares are most often used to find a local optimal solution; these belong, respectively, to the classes of derivative-free and derivative-based methods. For more details on local optimizers, the reader is referred to the books mentioned above.

By feasible point finders, we mean any method that can be used to correctly find a point $\mathbf{x}_f$ satisfying the following constraint:

$$g(\mathbf{x}_f) \leq 0, \quad \mathbf{x}_f \in \mathbb{X}. \tag{31}$$

A number of methods have been proposed to find a solution to (31) (see e.g. Polyak 1964; Pshenichnyi 1970; Robinson 1972; Daniel 1973; Dennis *et al.* 1999). These methods are of local nature and depend on a starting point. Thus there is no theoretical guarantee of finding a solution of (31). Recently, Xu (2003b) proposed a numerical method to find the smallest box(es) for bounding feasible points of (31). As a result of this development, we can always find a feasible point of (31) or conclude that (31) cannot be true for any point $\mathbf{x}$ in $\mathbb{X}$. Xu (2003b) has also shown that (31) is representative in the sense that a number of inequalities can be mathematically represented equivalently by (31).

In the 1-D case, the feasible point finder is simply equivalent to finding all the zero points of the equation

$$g(x) = 0, x \in [\underline{x}, \overline{x}], \tag{32}$$

where $\underline{x}$ and $\overline{x}$ are the lower and upper bounds of x, respectively. (32) can be solved by using the interval Newton method (e.g. Hansen 1992; Xu 2002). The multidimensional case is much more complicated and requires much more space to describe. Since the basic idea is the same as the 1-D case, we will not discuss it here. The interested reader should refer to Xu (2003a).

Now we are in a position to demonstrate how to assemble local optimizers and feasible point finders together and build up our hybrid global optimization algorithm. As the first step, one can apply a local optimization method to (29). We denote the local optimal solution set by $(\mathbf{x}_0^*, f_0^*)$. Then we can reformulate (29) as follows:

$$\text{min: } f(\mathbf{x}), \tag{33a}$$

subject to the constraint,

$$f(\mathbf{x}) \leq f_0^*, \mathbf{x} \in \mathbb{X}. \tag{33b}$$

Applying feasible point finders to (33b), we can then either obtain a feasible point $\mathbf{x}_f$ such that $f(\mathbf{x}_f) < f_0^*$ or find the global optimal solution(s). If the global optimal solution of (29) is unique, then we confirm at this step that $\mathbf{x}_0^*$ is globally optimal. Without loss of generality, assume that we do obtain a feasible point, say $\mathbf{x}_f$. Restarting the local optimizer from $\mathbf{x}_f$, we are assured of obtaining a better local solution set $(\mathbf{x}^*, f^*)$ such that $\mathbf{x}^* \neq \mathbf{x}_0^*$ and $f^* < f_0^*$. Replacing f_0^* with f^* in (33b), storing $\mathbf{x}^*$ as $\mathbf{x}_0^*$, and then repeating the above procedure, we guarantee theoretically that the global optimal solution(s) of (29) can always be found correctly. For more theoretical and technical details, the reader is referred to Xu (2002, 2003a,b).

APPENDIX B: THE BIASES OF THE FOUR STRESS PARAMETERS AND DERIVATIVES OF THE MAXIMUM SHEAR DIRECTIONS WITH RESPECT TO *D*

B1: The biases of the four stress parameters

Assume that the L_2-norm is used to (19). We have

$$\sum_{i=1}^{n} \dot{\mathbf{f}}_{id}^{\mathrm{T}}(\boldsymbol{\epsilon}_i, \hat{\mathbf{d}})\{\mathbf{s}_i(\boldsymbol{\epsilon}_i) - \mathbf{f}_i(\boldsymbol{\epsilon}_i, \hat{\mathbf{d}})\} = \mathbf{0}, \tag{34}$$

where

$$\mathbf{f}_i(\boldsymbol{\epsilon}_i, \hat{\mathbf{d}}) = \frac{\hat{\boldsymbol{D}}\mathbf{n}_i - (\mathbf{n}_i^{\mathrm{T}}\hat{\boldsymbol{D}}\mathbf{n}_i)\mathbf{n}_i}{\|\hat{\boldsymbol{D}}\mathbf{n}_i - (\mathbf{n}_i^{\mathrm{T}}\hat{\boldsymbol{D}}\mathbf{n}_i)\mathbf{n}_i\|},$$

$\hat{\mathbf{d}}$ stands for the estimate of $\mathbf{d}$. We use $\mathbf{s}_i(\boldsymbol{\varepsilon}_i)$ and $\mathbf{f}_i(\boldsymbol{\epsilon}_i, \hat{\mathbf{d}})$ to emphasize that the unit vectors $\mathbf{s}_i$ and f_i are functions of $\boldsymbol{\varepsilon}_i$, and $\boldsymbol{\varepsilon}_i$ and $\hat{\mathbf{d}}$, respectively.

In order to obtain a formula describing the biases of $\hat{\mathbf{d}}$, we have to expand all the terms in (34) up to the second order approximation at the points $\boldsymbol{\varepsilon}_i = \mathbf{0}$ and $\hat{\mathbf{d}} = \mathbf{d}$, as follows:

$$\mathbf{s}_i(\boldsymbol{\epsilon}_i) = \mathbf{s}_i + \dot{\mathbf{s}}_i\boldsymbol{\epsilon}_i + \frac{1}{2}\mathbf{G}_{s_i}\boldsymbol{\epsilon}_i, \tag{35a}$$

where

$$\mathbf{G}_{s_i} = \{\ddot{\mathbf{s}}_{1i}\boldsymbol{\epsilon}_i, \ddot{\mathbf{s}}_{2i}\boldsymbol{\epsilon}_i, \ddot{\mathbf{s}}_{3i}\boldsymbol{\epsilon}_i\}^{\mathrm{T}}.$$

$\mathbf{s}_i$, $\dot{\mathbf{s}}_i$ and $\ddot{\mathbf{s}}_{ji}$ are all computed at the point $\boldsymbol{\epsilon}_i = \mathbf{0}$. Similarly, we have

$$\dot{\mathbf{f}}_{id}(\boldsymbol{\epsilon}_i, \hat{\mathbf{d}}) = \dot{\mathbf{f}}_{id} + \begin{bmatrix} \boldsymbol{\epsilon}_i^{\mathrm{T}}\ddot{\mathbf{f}}_{1i\epsilon d} \\ \boldsymbol{\epsilon}_i^{\mathrm{T}}\ddot{\mathbf{f}}_{2i\epsilon d} \\ \boldsymbol{\epsilon}_i^{\mathrm{T}}\ddot{\mathbf{f}}_{3i\epsilon d} \end{bmatrix} + \begin{bmatrix} \mathbf{p}^{\mathrm{T}}\ddot{\mathbf{f}}_{1id} \\ \mathbf{p}^{\mathrm{T}}\ddot{\mathbf{f}}_{2id} \\ \mathbf{p}^{\mathrm{T}}\ddot{\mathbf{f}}_{3id} \end{bmatrix}, \tag{35b}$$

where $\mathbf{p} = \hat{\mathbf{d}} - \mathbf{d}$, $\mathbf{d}$ is the true but unknown vector of stress tensor parameters. $\dot{\mathbf{f}}_{id}$, $\ddot{\mathbf{f}}_{ji\epsilon d}$ and $\ddot{\mathbf{f}}_{jid}$ are all computed at the points $\boldsymbol{\epsilon}_i = \mathbf{0}$ and $\hat{\mathbf{d}} = \mathbf{d}$. Finally,

$$\mathbf{f}_i(\boldsymbol{\epsilon}_i, \hat{\mathbf{d}}) = \mathbf{f}_i + \dot{\mathbf{f}}_{i\epsilon}\boldsymbol{\epsilon}_i + \dot{\mathbf{f}}_{id}\mathbf{p} + \frac{1}{2}\begin{bmatrix} \boldsymbol{\epsilon}_i^{\mathrm{T}}\ddot{\mathbf{f}}_{1i\epsilon}\boldsymbol{\epsilon}_i + 2\boldsymbol{\epsilon}_i^{\mathrm{T}}\ddot{\mathbf{f}}_{1i\epsilon d}\mathbf{p} + \mathbf{p}^{\mathrm{T}}\ddot{\mathbf{f}}_{1id}\mathbf{p} \\ \boldsymbol{\epsilon}_i^{\mathrm{T}}\ddot{\mathbf{f}}_{2i\epsilon}\boldsymbol{\epsilon}_i + 2\boldsymbol{\epsilon}_i^{\mathrm{T}}\ddot{\mathbf{f}}_{2i\epsilon d}\mathbf{p} + \mathbf{p}^{\mathrm{T}}\ddot{\mathbf{f}}_{2id}\mathbf{p} \\ \boldsymbol{\epsilon}_i^{\mathrm{T}}\ddot{\mathbf{f}}_{3i\epsilon}\boldsymbol{\epsilon}_i + 2\boldsymbol{\epsilon}_i^{\mathrm{T}}\ddot{\mathbf{f}}_{3i\epsilon d}\mathbf{p} + \mathbf{p}^{\mathrm{T}}\ddot{\mathbf{f}}_{3id}\mathbf{p} \end{bmatrix}. \tag{35c}$$

Here $\mathbf{f}_i$ and all the derivatives of (35c) are computed at the same points.

If all the fault-slip data were without errors, then the estimate $\hat{\mathbf{d}}$ should reproduce $\mathbf{d}$ by minimizing (19). By Taylor-expanding $\mathbf{p}$ and truncating it at the second order approximation, we have

$$\mathbf{p} = \mathbf{H}\boldsymbol{\epsilon} + \mathbf{q}, \tag{36}$$

where $\mathbf{H}$ is a $(4 \times 3n)$ matrix to be determined,

$$\boldsymbol{\epsilon} = \left(\boldsymbol{\epsilon}_1^{\mathrm{T}}, \boldsymbol{\epsilon}_2^{\mathrm{T}}, \ldots, \boldsymbol{\epsilon}_n^{\mathrm{T}}\right)^{\mathrm{T}},$$

and

$$\mathbf{q} = \left(\boldsymbol{\epsilon}^{\mathrm{T}}\mathbf{M}_1\boldsymbol{\epsilon}, \boldsymbol{\epsilon}^{\mathrm{T}}\mathbf{M}_2\boldsymbol{\epsilon}, \boldsymbol{\epsilon}^{\mathrm{T}}\mathbf{M}_3\boldsymbol{\epsilon}, \boldsymbol{\epsilon}^{\mathrm{T}}\mathbf{M}_4\boldsymbol{\epsilon}\right)^{\mathrm{T}},$$

$\mathbf{M}_i (i = 1, 2, 3, 4)$ are four unknown symmetric matrices.

Inserting (35a), (35b), (35c) and (36) into (34), and putting all the linear terms of $\boldsymbol{\epsilon}$ together, we obtain

$$\sum_{i=1}^{n}\left\{\ddot{\mathbf{f}}_{id}^{\mathrm{T}}\dot{\mathbf{s}}_i\boldsymbol{\epsilon}_i-\ddot{\mathbf{f}}_{id}^{\mathrm{T}}\dot{\mathbf{f}}_{i\epsilon}\boldsymbol{\epsilon}_i-\ddot{\mathbf{f}}_{id}^{\mathrm{T}}\dot{\mathbf{f}}_{id}\mathbf{H}\boldsymbol{\epsilon}\right\}=\mathbf{0},$$

from which we can immediately find $\mathbf{H}$ as follows:

$$\mathbf{H}=\left(\sum_{i=1}^{n}\ddot{\mathbf{f}}_{id}^{\mathrm{T}}\dot{\mathbf{f}}_{id}\right)^{-1}\left\{\ddot{\mathbf{f}}_{1d}^{\mathrm{T}}(\dot{\mathbf{s}}_1-\dot{\mathbf{f}}_{1\epsilon}),\ddot{\mathbf{f}}_{2d}^{\mathrm{T}}(\dot{\mathbf{s}}_2-\dot{\mathbf{f}}_{2\epsilon}),\ldots,\ddot{\mathbf{f}}_{nd}^{\mathrm{T}}(\dot{\mathbf{s}}_n-\dot{\mathbf{f}}_{n\epsilon})\right\}. \tag{37}$$

Similarly, by putting all the quadratic terms of $\boldsymbol{\epsilon}$ together and after some derivations and rearrangement, we obtain

$$\mathbf{q}=\left(\sum_{i=1}^{n}\ddot{\mathbf{f}}_{id}^{\mathrm{T}}\dot{\mathbf{f}}_{id}\right)^{-1}(\mathbf{q}_s+\mathbf{q}_{f\epsilon}+\mathbf{q}_{fd}+\mathbf{q}_{f\epsilon d}), \tag{38}$$

where

$$\mathbf{q}_s=\frac{1}{2}\sum_{i=1}^{n}\ddot{\mathbf{f}}_{id}^{\mathrm{T}}\begin{bmatrix}\boldsymbol{\epsilon}_i^{\mathrm{T}}\ddot{\mathbf{s}}_{1i}\boldsymbol{\epsilon}_i\\ \boldsymbol{\epsilon}_i^{\mathrm{T}}\ddot{\mathbf{s}}_{2i}\boldsymbol{\epsilon}_i\\ \boldsymbol{\epsilon}_i^{\mathrm{T}}\ddot{\mathbf{s}}_{3i}\boldsymbol{\epsilon}_i\end{bmatrix}, \tag{39a}$$

$$\mathbf{q}_{f\epsilon}=-\frac{1}{2}\sum_{i=1}^{n}\ddot{\mathbf{f}}_{id}^{\mathrm{T}}\begin{bmatrix}\boldsymbol{\epsilon}_i^{\mathrm{T}}\ddot{\mathbf{f}}_{1i\epsilon}\boldsymbol{\epsilon}_i\\ \boldsymbol{\epsilon}_i^{\mathrm{T}}\ddot{\mathbf{f}}_{2i\epsilon}\boldsymbol{\epsilon}_i\\ \boldsymbol{\epsilon}_i^{\mathrm{T}}\ddot{\mathbf{f}}_{3i\epsilon}\boldsymbol{\epsilon}_i\end{bmatrix}, \tag{39b}$$

$$\mathbf{q}_{fd}=-\frac{1}{2}\sum_{i=1}^{n}\ddot{\mathbf{f}}_{id}^{\mathrm{T}}\begin{bmatrix}\boldsymbol{\epsilon}^{\mathrm{T}}\mathbf{H}^{\mathrm{T}}\ddot{\mathbf{f}}_{1id}\mathbf{H}\boldsymbol{\epsilon}\\ \boldsymbol{\epsilon}^{\mathrm{T}}\mathbf{H}^{\mathrm{T}}\ddot{\mathbf{f}}_{2id}\mathbf{H}\boldsymbol{\epsilon}\\ \boldsymbol{\epsilon}^{\mathrm{T}}\mathbf{H}^{\mathrm{T}}\ddot{\mathbf{f}}_{3id}\mathbf{H}\boldsymbol{\epsilon}\end{bmatrix}-\sum_{i=1}^{n}\begin{bmatrix}\boldsymbol{\epsilon}^{\mathrm{T}}\mathbf{H}^{\mathrm{T}}\ddot{\mathbf{f}}_{1id}\\ \boldsymbol{\epsilon}^{\mathrm{T}}\mathbf{H}^{\mathrm{T}}\ddot{\mathbf{f}}_{2id}\\ \boldsymbol{\epsilon}^{\mathrm{T}}\mathbf{H}^{\mathrm{T}}\ddot{\mathbf{f}}_{3id}\end{bmatrix}^{\mathrm{T}}\dot{\mathbf{f}}_{id}\mathbf{H}\boldsymbol{\epsilon}+\sum_{i=1}^{n}\begin{bmatrix}\boldsymbol{\epsilon}^{\mathrm{T}}\mathbf{H}^{\mathrm{T}}\ddot{\mathbf{f}}_{1id}\\ \boldsymbol{\epsilon}^{\mathrm{T}}\mathbf{H}^{\mathrm{T}}\ddot{\mathbf{f}}_{2id}\\ \boldsymbol{\epsilon}^{\mathrm{T}}\mathbf{H}^{\mathrm{T}}\ddot{\mathbf{f}}_{3id}\end{bmatrix}^{\mathrm{T}}\dot{\mathbf{s}}_i\boldsymbol{\epsilon}_i-\sum_{i=1}^{n}\begin{bmatrix}\boldsymbol{\epsilon}^{\mathrm{T}}\mathbf{H}^{\mathrm{T}}\ddot{\mathbf{f}}_{1id}\\ \boldsymbol{\epsilon}^{\mathrm{T}}\mathbf{H}^{\mathrm{T}}\ddot{\mathbf{f}}_{2id}\\ \boldsymbol{\epsilon}^{\mathrm{T}}\mathbf{H}^{\mathrm{T}}\ddot{\mathbf{f}}_{3id}\end{bmatrix}^{\mathrm{T}}\dot{\mathbf{f}}_{i\epsilon}\boldsymbol{\epsilon}_i, \tag{39c}$$

$$\mathbf{q}_{f\epsilon d}=\sum_{i=1}^{n}\begin{bmatrix}\boldsymbol{\epsilon}_i^{\mathrm{T}}\ddot{\mathbf{f}}_{1i\epsilon d}[\\ \boldsymbol{\epsilon}_i^{\mathrm{T}}\ddot{\mathbf{f}}_{2i\epsilon d}[\\ \boldsymbol{\epsilon}_i^{\mathrm{T}}\ddot{\mathbf{f}}_{3i\epsilon d}[\end{bmatrix}^{\mathrm{T}}\dot{\mathbf{s}}_i\boldsymbol{\epsilon}_i-\sum_{i=1}^{n}\ddot{\mathbf{f}}_{id}^{\mathrm{T}}\begin{bmatrix}\boldsymbol{\epsilon}_i^{\mathrm{T}}\ddot{\mathbf{f}}_{1i\epsilon d}\mathbf{H}\boldsymbol{\epsilon}\\ \boldsymbol{\epsilon}_i^{\mathrm{T}}\ddot{\mathbf{f}}_{2i\epsilon d}\mathbf{H}\boldsymbol{\epsilon}\\ \boldsymbol{\epsilon}_i^{\mathrm{T}}\ddot{\mathbf{f}}_{3i\epsilon d}\mathbf{H}\boldsymbol{\epsilon}\end{bmatrix}-\sum_{i=1}^{n}\begin{bmatrix}\boldsymbol{\epsilon}_i^{\mathrm{T}}\ddot{\mathbf{f}}_{1i\epsilon d}\\ \boldsymbol{\epsilon}_i^{\mathrm{T}}\ddot{\mathbf{f}}_{2i\epsilon d}\\ \boldsymbol{\epsilon}_i^{\mathrm{T}}\ddot{\mathbf{f}}_{3i\epsilon d}\end{bmatrix}^{\mathrm{T}}(\dot{\mathbf{f}}_{i\epsilon}\boldsymbol{\epsilon}_i+\dot{\mathbf{f}}_{id}\mathbf{H}\boldsymbol{\epsilon}). \tag{39d}$$

The biases of the four estimated stress parameters $\hat{\mathbf{d}}$ can now be readily obtained by applying the expectation operator to $\mathbf{q}$, namely,

$$\begin{aligned}\mathbf{b}(\hat{\mathbf{d}})&=E(\hat{\mathbf{d}}-\mathbf{d})=E(\mathbf{q})\\&=\left(\sum_{i=1}^{n}\ddot{\mathbf{f}}_{id}^{\mathrm{T}}\dot{\mathbf{f}}_{id}\right)^{-1}(\mathbf{b}_s+\mathbf{b}_{f\epsilon}+\mathbf{b}_{fd}+\mathbf{b}_{f\epsilon d}),\end{aligned} \tag{40a}$$

where

$$\mathbf{b}_s=E(\mathbf{q}_s)=\frac{1}{2}\sum_{i=1}^{n}\ddot{\mathbf{f}}_{id}^{\mathrm{T}}\begin{bmatrix}\mathrm{tr}\{\ddot{\mathbf{s}}_{1i}\mathbf{V}_i\}\\ \mathrm{tr}\{\ddot{\mathbf{s}}_{2i}\mathbf{V}_i\}\\ \mathrm{tr}\{\ddot{\mathbf{s}}_{3i}\mathbf{V}_i\}\end{bmatrix}, \tag{40b}$$

$$\mathbf{b}_{f\epsilon}=E(\mathbf{q}_{f\epsilon})=-\frac{1}{2}\sum_{i=1}^{n}\ddot{\mathbf{f}}_{id}^{\mathrm{T}}\begin{bmatrix}\mathrm{tr}\{\ddot{\mathbf{f}}_{1i\epsilon}\mathbf{V}_i\}\\ \mathrm{tr}\{\ddot{\mathbf{f}}_{2i\epsilon}\mathbf{V}_i\}\\ \mathrm{tr}\{\ddot{\mathbf{f}}_{3i\epsilon}\mathbf{V}_i\}\end{bmatrix}, \tag{40c}$$

$$\begin{aligned}\mathbf{b}_{fd}=E(\mathbf{q}_{fd})=&-\frac{1}{2}\sum_{i=1}^{n}\ddot{\mathbf{f}}_{id}^{\mathrm{T}}\begin{bmatrix}\mathrm{tr}\left\{\mathbf{H}^{\mathrm{T}}\ddot{\mathbf{f}}_{1id}\mathbf{H}\mathbf{V}\right\}\\ \mathrm{tr}\left\{\mathbf{H}^{\mathrm{T}}\ddot{\mathbf{f}}_{2id}\mathbf{H}\mathbf{V}\right\}\\ \mathrm{tr}\left\{\mathbf{H}^{\mathrm{T}}\ddot{\mathbf{f}}_{3id}\mathbf{H}\mathbf{V}\right\}\end{bmatrix}-\sum_{i=1}^{n}\begin{bmatrix}\ddot{\mathbf{f}}_{1id}\\ \ddot{\mathbf{f}}_{2id}\\ \ddot{\mathbf{f}}_{3id}\end{bmatrix}^{\mathrm{T}}\mathrm{vec}\left\{\mathbf{H}\mathbf{V}\mathbf{H}^{\mathrm{T}}\ddot{\mathbf{f}}_{id}^{\mathrm{T}}\right\}\\&+\sum_{i=1}^{n}\begin{bmatrix}\ddot{\mathbf{f}}_{1id}\\ \ddot{\mathbf{f}}_{2id}\\ \ddot{\mathbf{f}}_{3id}\end{bmatrix}^{\mathrm{T}}\mathrm{vec}\left\{\mathbf{H}_i\mathbf{V}_i\dot{\mathbf{s}}_i^{\mathrm{T}}\right\}-\sum_{i=1}^{n}\begin{bmatrix}\ddot{\mathbf{f}}_{1id}\\ \ddot{\mathbf{f}}_{2id}\\ \ddot{\mathbf{f}}_{3id}\end{bmatrix}^{\mathrm{T}}\mathrm{vec}\left\{\mathbf{H}_i\mathbf{V}_i\dot{\mathbf{f}}_{i\epsilon}^{\mathrm{T}}\right\},\end{aligned} \tag{40d}$$

$$\mathbf{b}_{f\epsilon d} = E(\mathbf{q}_{f\epsilon d}) = \sum_{i=1}^{n} \begin{bmatrix} \ddot{\mathbf{f}}_{1i\epsilon d} \\ \ddot{\mathbf{f}}_{2i\epsilon d} \\ \ddot{\mathbf{f}}_{3i\epsilon d} \end{bmatrix}^{\mathrm{T}} \mathrm{vec}\left\{\mathbf{V}_i \dot{\mathbf{s}}_i^{\mathrm{T}}\right\} - \sum_{i=1}^{n} \dot{\mathbf{f}}_{id}^{\mathrm{T}} \begin{bmatrix} \mathrm{tr}\{\ddot{\mathbf{f}}_{1i\epsilon d}\mathbf{H}_i\mathbf{V}_i\} \\ \mathrm{tr}\{\ddot{\mathbf{f}}_{2i\epsilon d}\mathbf{H}_i\mathbf{V}_i\} \\ \mathrm{tr}\{\ddot{\mathbf{f}}_{3i\epsilon d}\mathbf{H}_i\mathbf{V}_i\} \end{bmatrix} - \sum_{i=1}^{n} \begin{bmatrix} \ddot{\mathbf{f}}_{1i\epsilon d} \\ \ddot{\mathbf{f}}_{2i\epsilon d} \\ \ddot{\mathbf{f}}_{3i\epsilon d} \end{bmatrix}^{\mathrm{T}} \mathrm{vec}\left\{\mathbf{V}_i\left(\dot{\mathbf{f}}_{i\epsilon}^{\mathrm{T}} + \mathbf{H}_i^{\mathrm{T}}\dot{\mathbf{f}}_{id}^{\mathrm{T}}\right)\right\}, \tag{40e}$$

and

$$\mathbf{V} = \mathrm{diag}(\mathbf{V}_i), \tag{40f}$$

$$\mathbf{H}_i = \left(\sum_{i=1}^{n} \dot{\mathbf{f}}_{id}^{\mathrm{T}}\dot{\mathbf{f}}_{id}\right)^{-1} \dot{\mathbf{f}}_{id}^{\mathrm{T}}(\dot{\mathbf{s}}_i - \dot{\mathbf{f}}_{i\epsilon}). \tag{40g}$$

Here $\mathrm{tr}\{\mathbf{A}\}$ stands for the trace of the matrix $\mathbf{A}$, and $\mathrm{vec}\{\mathbf{A}\}$ for the vectorizing operation of $\mathbf{A}$.

B2. Derivatives of the maximum shear directions with respect to d

Substituting the reduced deviatoric stress tensor $\boldsymbol{D}$ of (9) into (4), we obtain after some derivations

$$\mathbf{f}_s = \mathbf{C}\mathbf{d}_5, \tag{41}$$

for each fault, where

$\mathbf{d}_5 = (\cos\varphi, \sin\varphi, \alpha, \beta, \gamma)^{\mathrm{T}}$,

and the matrix $\mathbf{C}$ is given as follows:

$$\mathbf{C} = \begin{bmatrix} -\frac{1}{2}n_x\left(2n_x^2 - n_y^2 - n_z^2 - 2\right) & \frac{\sqrt{3}}{2}n_x\left(n_y^2 - n_z^2\right) & n_y\left(1 - 2n_x^2\right) & -2n_x n_y n_z & n_z\left(1 - 2n_x^2\right) \\ -\frac{1}{2}n_y\left(2n_x^2 - n_y^2 - n_z^2 + 1\right) & \frac{\sqrt{3}}{2}n_y\left(n_y^2 - n_z^2 - 1\right) & n_x\left(1 - 2n_y^2\right) & n_z\left(1 - 2n_y^2\right) & -2n_x n_y n_z \\ -\frac{1}{2}n_z\left(2n_x^2 - n_y^2 - n_z^2 + 1\right) & \frac{\sqrt{3}}{2}n_z\left(n_y^2 - n_z^2 + 1\right) & -2n_x n_y n_z & n_y\left(1 - 2n_z^2\right) & n_x\left(1 - 2n_z^2\right) \end{bmatrix}. \tag{42}$$

For each of the three components of the normalized unit vector of the maximum shear stress $\mathbf{f}_{\mathrm{s}}$, we obtain its derivatives with respect to the four stress parameters:

$$\frac{\partial f_{\mathrm{sn}}^i}{\partial\varphi} = \frac{c_{i2}\cos\varphi - c_{i1}\sin\varphi}{\|\mathbf{C}\mathbf{d}_5\|^{1/2}} - \frac{(\mathbf{c}_i\mathbf{d}_5)\left(\sum_{j=1}^{3} c_{j2}\cos\varphi - \sum_{j=1}^{3} c_{j1}\sin\varphi\right)}{\|\mathbf{C}\mathbf{d}_5\|^{3/2}}, \tag{43a}$$

$$\frac{\partial f_{\mathrm{sn}}^i}{\partial\alpha} = \frac{c_{i3}}{\|\mathbf{C}\mathbf{d}_5\|^{1/2}} - \frac{(\mathbf{c}_i\mathbf{d}_5)\sum_{j=1}^{3} c_{j3}}{\|\mathbf{C}\mathbf{d}_5\|^{3/2}}, \tag{43b}$$

$$\frac{\partial f_{\mathrm{sn}}^i}{\partial\beta} = \frac{c_{i4}}{\|\mathbf{C}\mathbf{d}_5\|^{1/2}} - \frac{(\mathbf{c}_i\mathbf{d}_5)\sum_{j=1}^{3} c_{j4}}{\|\mathbf{C}\mathbf{d}_5\|^{3/2}}, \tag{43c}$$

$$\frac{\partial f_{\mathrm{sn}}^i}{\partial\gamma} = \frac{c_{i5}}{\|\mathbf{C}\mathbf{d}_5\|^{1/2}} - \frac{(\mathbf{c}_i\mathbf{d}_5)\sum_{j=1}^{3} c_{j5}}{\|\mathbf{C}\mathbf{d}_5\|^{3/2}}. \tag{43d}$$

Here i stands for the ith component of $\mathbf{f}_{\mathrm{ns}}$, $\mathbf{c}_i$ is the ith row of $\mathbf{C}$, and $c_{ij}(i = 1, 2, 3;\ j = 1, 2, \ldots, 5)$ are the elements of $\mathbf{C}$.